Building and Environment 295 (2026) 114434

Contents lists available at ScienceDirect

Building and Environment

journal homepage: www.elsevier.com/locate/buildenv

Thermal comfort on the move: Understanding thermal alliesthesia on urban walking routes

Yichun Li [a], Xianzhun Zhong [a], Yongxin Xie [a,*], Richard de Dear [b], Shuai Lu [c], Borong Lin [d], Jianlei Niu [a]

[a] Department of Building Environment and Energy Engineering, The Hong Kong Polytechnic University, Hung Hom, Kowloon, Hong Kong
[b] School of Architecture, Design and Planning, the University of Sydney, NSW, Australia
[c] Shenzhen International Graduate School, Tsinghua University, Shenzhen, Guangdong 518055, China
[d] Department of Building Science, School of Architecture, Tsinghua University, Beijing, 100084, China

ARTICLE INFO

Keywords:
Dynamic outdoor thermal comfort
Human body thermal storage
Thermal alliesthesia
Spatial alliesthesia
Temporal alliesthesia

ABSTRACT

Walking outdoors exposes pedestrians in urban settings to diverse and complex sequences of microclimates which can potentially prompt experiences of thermal alliesthesia: transient feelings of thermal pleasure (positive alliesthesia) or discomfort (negative alliesthesia). While adventitious spatial microclimatic variations hold potential to enhance pedestrian thermal comfort, their practical application in urban design contexts remains underexplored in the literature to date. This study investigates how thermal alliesthesia can be leveraged to enhance the subjective thermal experiences of urban pedestrians. To address this question, 51 human subjects were recruited to walk along a designated outdoor route in Beijing, specifically selected to present thermal transitions that could potentially stimulate thermal alliesthesia during winter, spring and summer. As the residual heat accumulating in or depleting from body tissue when its heat inputs and outputs are unbalanced, thermal storage (*TS*) is utilized to characterize the objective thermal status within the human body and quantify the boundaries of the thermoneutral zone. Results identified a moderate thermal alliesthesia potential zone within the range of 8.05–93.23 W/m^2 thermal storage. Within this zone, the variations of *TS* and thermal comfort vote (*TCV*) follow a quadratic relationship, while in strong thermal alliesthesia potential zones, they follow a linear relationship. Both temporal and spatial variations in thermal conditions influence *TCV*. This study demonstrates how spatial microclimatic variations can be curated to enrich the subjective experience of pedestrians in urban settings, providing a framework for purposively applying thermal alliesthesia principles in urban design and pedestrian environments.

1. Introduction

1.1. General background

The extreme weather conditions resulting from global warming are being superimposed on the urban heat island effect, and the combined effect is significantly deterring city dwellers from engaging in outdoor activities [1]. However, outdoor thermal experiences are a key element of low-carbon urban lifestyles [2] and cities' long-term sustainability [3]. Current urban pedestrian space planning primarily focuses on functional aspects, often neglecting the actual thermal environments experienced by pedestrians [4]. Pedestrians are inevitably exposed to diverse urban morphologies resulting in complex shade distributions, street geometries, proximity to water bodies, etc., all of which result in a variety of wind and radiation environments for the pedestrian [5–7]. In summary, to effectively remediate overheated urban biometeorological environments and improve the subjective comfort perceptions of pedestrians, it is essential to develop a more detailed and comprehensive understanding of how these outdoor environmental factors interact to affect thermal perception and the walkability of urban landscapes [8].

1.2. How dynamic thermal exposure shapes pedestrian's thermal perceptions

Fig. 1 illustrates the heat exchange between pedestrians and the environment during outdoor walking. Pedestrian thermal perception is shaped by air temperature, humidity, wind speed, and solar radiation,

* Corresponding author.
E-mail address: yongxxie@polyu.edu.hk (Y. Xie).

https://doi.org/10.1016/j.buildenv.2026.114434
Received 17 December 2025; Received in revised form 25 February 2026; Accepted 28 February 2026
Available online 28 February 2026

Nomenclature

a_k	Absorption coefficient for short-wave radiation
BSA	Body surface area m^2
BSA_i	Local body surface area m^2
BSA_{ra}	Ratio of body surface area to standard body surface area-
BSA_{st}	Body surface area of the standard body m^2
C	Rate of convective heat loss W/m^2
$dTAV$	Changes in thermal acceptability vote
$dTCV$	Changes in thermal comfort vote
dTS	Changes in thermal storage W/m^2
$dTSV$	Changes in thermal sensation vote
E_{sk}	Rate of evaporative heat loss from the skin W/m^2
f_a	Solid angle factor for the upward and downward hemispheres-
$f_{base_{cr},i}$	Distribution coefficient of heat production from core
$f_{base_{fat,i}}$	Distribution coefficient of heat production from fat
$f_{base_{ms,i}}$	Distribution coefficient of heat production from muscle
$f_{base_{sk,i}}$	Distribution coefficient of heat production from skin-
f_{cl}	Clothing area factor that accounts for the increased area due to clothing-
$f_{cl,i}$	The local clothing area factor
$h_{c,i}$	Convective heat transfer coefficient $W/m^2 \cdot K$
$h_{et,i}$	Local evaporative heat transfer coefficient $W/m^2 \cdot K$
$h_{r,i}$	Radiative heat transfer coefficient $W/m^2 \cdot K$
$h_{t,i}$	Sensible heat transfer coefficient $W/m^2 \cdot K$
I_{cl}	Thermal resistance of clothing $(m^2 \cdot K)/W$
L_R	Lewis constant K/kPa
M	Rate of metabolic heat production W/m^2
M_{base_all}	Basal metabolism in whole body W
$M_{base,i}$	Heat production by local basal metabolism for each body segment W
$M_{base_{cr,i}}$	Local heat production from core W
$M_{base_{fat,i}}$	Local heat production from fat W
M_{base}	Local heat production by basal metabolism W
$M_{base_{ms,i}}$	Local heat production from muscle W
$M_{base_{sk,i}}$	Local heat production from skin W
M_i	Local metabolic heat production rate for each body segment W/m^2
$M_{work,i}$	Local heat production by external work W
p_a	Water vapor pressure in ambient air kPa
PAR	Physical activity ratio
$p_{sk,s,i}$	Saturated water vapor pressure at the skin kPa
Q_{lw-d}	Downward long-wave radiation W/m^2
Q_{lw-u}	Upward long-wave radiation W/m^2
Q_{res}	Rate of respiratory heat loss W/m^2
Q_{sw-d}	Downward short-wave radiation W/m^2
Q_{sw-u}	Upward short-wave radiation W/m^2
RH	Relative humidity %
R_L	Rate of long-wave radiative heat loss W/m^2
R_S	Rate of short-wave radiative heat gain W/m^2
s_i	Short-wave radiation intensity W/m^2
T_a	Air temperature °C
TCV_mean	Overall TCV
TI	Turbulence intensity
TS	Thermal storage per unit of skin area W/m^2
TS_mean	Overall thermal storage W/m^2
TS_{p_n}	Thermal storage at the current location W/m^2
$TS_{p_{n-1}}$	Thermal storage at the previous location W/m^2
TS_{prefer}	Preferred thermal storage W/m^2
TS_{t_1}	Thermal storage at t_1 W/m^2
TS_{t_0}	Thermal storage at t_0 W/m^2
ΔTS	TS variation values W/m^2
T_{mrt}	Mean radiant temperature °C
$T_{o,i}$	Operative temperature °C
T_{shiv}	Core temperature of head at the onset of shivering °C
T_{sk}	Skin Temperature °C
$T_{sk,i}$	Local skin surface temperature °C
$T_{sk,m}$	Mean skin temperature °C
T_{sr}	Surface temperature of the surroundings °C
t_0	Time used for calculation
t_1	Time of questionnaire submission-
v	Relevant wind speed m/s
W	Rate of mechanical work accomplished W/m^2
α	Azimuth angle °
β	Altitude angle °
ε_p	Emissivity of the clothed human body for long-wave radiation -
σ	Stefan–Boltzmann constant $W/(m^2K^4)$
ω_i	Local skin wetness

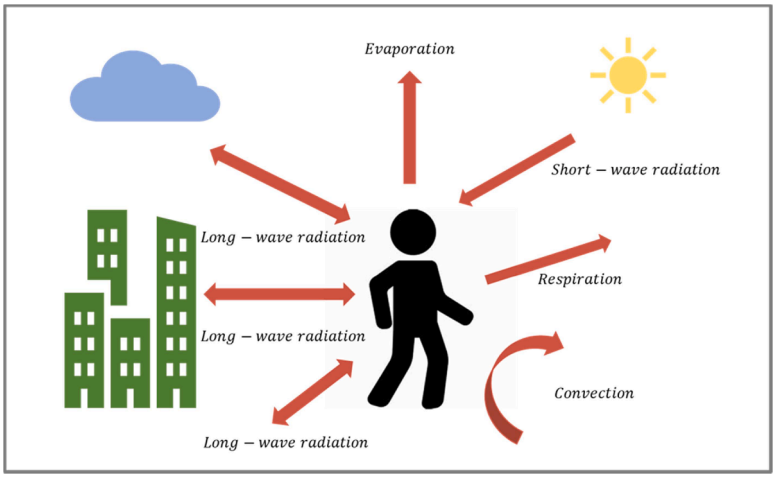

Fig. 1. Heat transfer between pedestrians and environment (modified after [12]).

which together regulate heat exchange at the skin surface [9]. Variations in walking speeds result in different relative wind speeds, generating dynamic thermal stimuli that alter pedestrians' satisfaction [10], while the sequence of exposed conditions and the direction of thermal transients significantly influence pedestrians' thermal perceptions [11].

Therefore, deliberately designing and curating thermal environmental scenarios for pedestrians in urban settings is becoming increasingly important [13,14]. Current strategies improve thermal comfort through vegetation transpiration, localized shade (urban green infrastructure) [15,16] or evaporative cooling (water bodies) [17,18]. However, these approaches often address environmental variables in isolation, despite the fact that outdoor biometeorological factors interact and jointly shape pedestrian thermal experience [19]. Also, interventions typically focus on improving microclimates at fixed locations, while overlooking the continuous and dynamic exposure to varying thermal environments that pedestrians experience along an entire walking route [20]. These limitations highlight the need to consider pedestrian thermal experience as a dynamic process that unfolds continuously along the walking route, rather than as a series of static microclimatic conditions.

Dynamic microclimatic variations along pedestrian routes, including sunshade alternations and intermittent exposures to different thermal stimuli, influence thermal perception beyond instantaneous conditions [21]. Traditional static monitoring methods are insufficient to capture pedestrian-scale dynamic changes in radiation and airflow [22]. These transient experiences accumulate over time, meaning thermal sensation is determined by the integral of stimulus intensity and duration rather than instantaneous values [23,24]. Beyond external exposure, such cumulative thermal experiences interact with the pedestrian's internal thermophysiological state, which is itself subject to continuous change during walking. Furthermore, the pedestrian's internal thermal state is inherently non-steady. Unlike sedentary subjects, pedestrians experience continuous metabolic fluctuations. Experimental studies indicate that although metabolic rate typically stabilizes within several minutes following changes in activity level, subjective thermal sensation exhibits a much longer temporal lag [25]. This temporal mismatch leads to a dual response pattern, in which activity level substantially modulates human sensitivity to step changes in environmental thermal conditions [26]. As a result, thermal comfort under dynamic conditions cannot be explained solely by physiological adjustment but also depends on subjective responses to thermal change.

Physiological responses and psychological thermal perception are often asynchronous under dynamic conditions. Transient thermal exposures can induce overshoot responses in thermal sensations that are not synchronized with skin temperature changes, reflecting a temporal mismatch between thermoregulation and perception [27,28]. This mismatch is especially evident during environmental transitions and creates conditions under which thermal stimuli may be perceived as pleasant when they contribute to restoring internal thermal balance. Such responses are consistent with the concept of thermal alliesthesia and suggest that it can be deliberately exploited to enhance pedestrian thermal experience in urban environments [10].

1.3. Potential application of thermal alliesthesia in enhancing urban pedestrian thermal comfort

Natural fluctuations in outdoor thermal environments offer significant potential for the application of thermal alliesthesia in improving outdoor thermal comfort. This concept originated from the broader concept of "alliesthesia", initially proposed by Cabanac in 1971 [29]. It refers to the phenomenon of how identical environmental stimuli can be perceived as pleasant or unpleasant, depending on the body's current needs and physiological status [30]. According to its original definition, pleasure arises when an external stimulus has the potential to restore the regulated variable within the *milieu interieur* to its set-point, hence cold stimuli are perceived as pleasant by a hyperthermic subject, and warm stimuli feel pleasant to their hypothermic counterpart. Conversely, thermal displeasure (negative alliesthesia) is experienced whenever a stimulus challenges the subject's homeothermic balance [31].

Thermal alliesthesia has been classified into both temporal and spatial variants [37]. Temporal alliesthesia results from environmental temperature step-changes, ramps and drifts [32], while spatial alliesthesia can be caused by localized cooling or heating of specific regions of skin [31–34]. Based on the mechanisms of spatial and temporal thermal alliesthesia, triggering pleasant, positive alliesthesia can be a useful strategy to improve thermal comfort. In indoor scenarios, the predominant approach is to utilize Personal Comfort Systems (*PCS*) to deliver rapid or targeted thermal stimuli to specific human body segments, leading to intense feelings of pleasure [35]. For example, He et al. [36] demonstrated that rapid whole-body warming followed by sustained local heating can induce both temporal and spatial alliesthesia under cold conditions. Watanabe et al. [37] showed that localized infrared radiation applied to the skin can elicit spatial alliesthesia through rapid increases in local skin temperature. Similarly, Belyamani et al. [38] reported positive alliesthesia effects using wearable thermoelectric modules to provide localized skin cooling. These experimental protocols serve as evidence supporting the notion that both temporal and spatial alliesthesia have the capacity to trigger thermal pleasure.

Compared with the static and spatially uniform biometeorological conditions typically found inside built environments, outdoor thermal environments present more diverse opportunities for thermal alliesthesia [39]. It was observed that thermal alliesthesia enhanced the thermal pleasure experienced during outdoor walking [40]. In semi-outdoor spaces, the uphill walking experiment conducted by Smail et al. [41] used fatigue as an indicator of thermal discomfort. This urban experiment was conducted in the winter and summer afternoons in the Mediterranean climate of Algiers' Casbah city, confirming that prolonged exposure to solar radiation accumulates thermal storage in body tissue, leading to negative alliesthesia and intensifying fatigue. In contrast, pedestrians can experience restorative effects after short-term exposure to intermittent shade and ventilated passages, triggering positive alliesthesia and mitigating fatigue and the associated thermal discomfort [41]. Zhang et al. [10] have conducted an outdoor walking experiment on a urban university campus. The experiment was carried out during daytime in summer under a humid subtropical climate. The subjects' perambulations disturbed the wind field around their bodies, and the resultant air motion at their skin surface was identified as the primary driver of both temporal and spatial thermal alliesthesia. Variations in different wind speeds can either increase or decrease pedestrians' thermal pleasure, which can be considered as a potential way of applying thermal alliesthesia in enhancing thermal experiences.

To more fully realise the potential for thermal alliesthesia to enhance thermal comfort and pleasure experienced during outdoor walking, both qualitative and quantitative research is needed. Parkinson and de Dear [31] proposed a conceptual framework of thermal alliesthesia that classifies the potential for thermal alliesthesia based upon the subject's physiological status relative to the thermoneutral zone of thermoregulation. The framework was divided into three zones based on the potential for triggering alliesthesia: the thermoneutral zone in which vasomotion is the primary effector mechanism of thermal regulation, metabolic regulatory zone (shivering), and sudomotor regulatory zone (sweating). The potential for alliestheia was proportional to the subject's physiological divergence from thermal thermoneutral zone. Subsequently, the framework was elaborated into five distinct zones, each associated with different thermal perceptions [33]: cold discomfort, acceptably cool, preferable, acceptably warm, and warm discomfort. As a qualitative framework, this nomenclature was applied to dynamic thermal pleasure in non-steady environments [42]. Several researchers have attempted to conduct quantitative analyses of outdoor thermal alliesthesia. Liu et al. [43] first attempted a quantitive thermal biometeorological lexicon by associating different thermal sensation scales into four zones of alliesthesial potential based on their divergence from

the preferred thermal sensation. The relationship between changes in thermal sensation and thermal pleasure was further explored within different alliesthesial zones. Jiang et al. [27] substituted thermal pleasure with thermal comfort, and examined the relationship between changes in thermal sensation and changes in thermal comfort within these four zones.

From these studies of the language of thermal alliesthesia it becomes clear that there are certain limitations in applying the purely descriptive language of the classic thermal sensation scale to characterize the affective or hedonic experience of spatial temporal alliesthesia in outdoor settings. On the one hand, individual perceptions of thermal sensation can be biased [44]. For instance, as one approaches the thermal natural zone, the distinctions between "slightly cool" and "slightly warm" compared to "neutral" can become blurred [45]. Also, when unable to alter their physiological status, people may adapt their perception of thermal neutrality by raising the discomfort threshold, bringing their current status within the widened scope of subjective thermal neutrality [46]. A more objective parameter is needed to more precisely quantify the alliesthesial framework and facilitate its applicability in the design and management of the thermal environments in semi-outdoor and outdoor contexts. Thermal storage (*TS*) in body tissuecould potentially serve this purpose. *TS* objectively quantifies one's thermal status by measuring the residual heat stored in the body when heat transfers into and out from the body are imbalanced. It takes full account of metabolic heat production, external work performed, longwave and shortwave radiation fluxes, convective and latent heat fluxes, as well as conductive heat transfers across the surface area of the body [47].

1.4. Research objectives

In this study, human body thermal storage is utilized to quantify thermal alliesthesia potential and to examine its relationship with pedestrians' subjective thermal comfort.

The specific objectives are as follows:

1. To quantitatively classify the alliesthesial framework based on thermal storage and explore the relationship between changes of thermal storage and thermal comfort cross different zones of alliesthesial potential;
2. To investigate how temporal alliesthesia affects pedestrian thermal comfort and examine how the amounts of thermal storage accumulated from preceding thermal exposures affect current subjective thermal comfort status;
3. To investigate the impact of spatial alliesthesia on pedestrian thermal comfort.

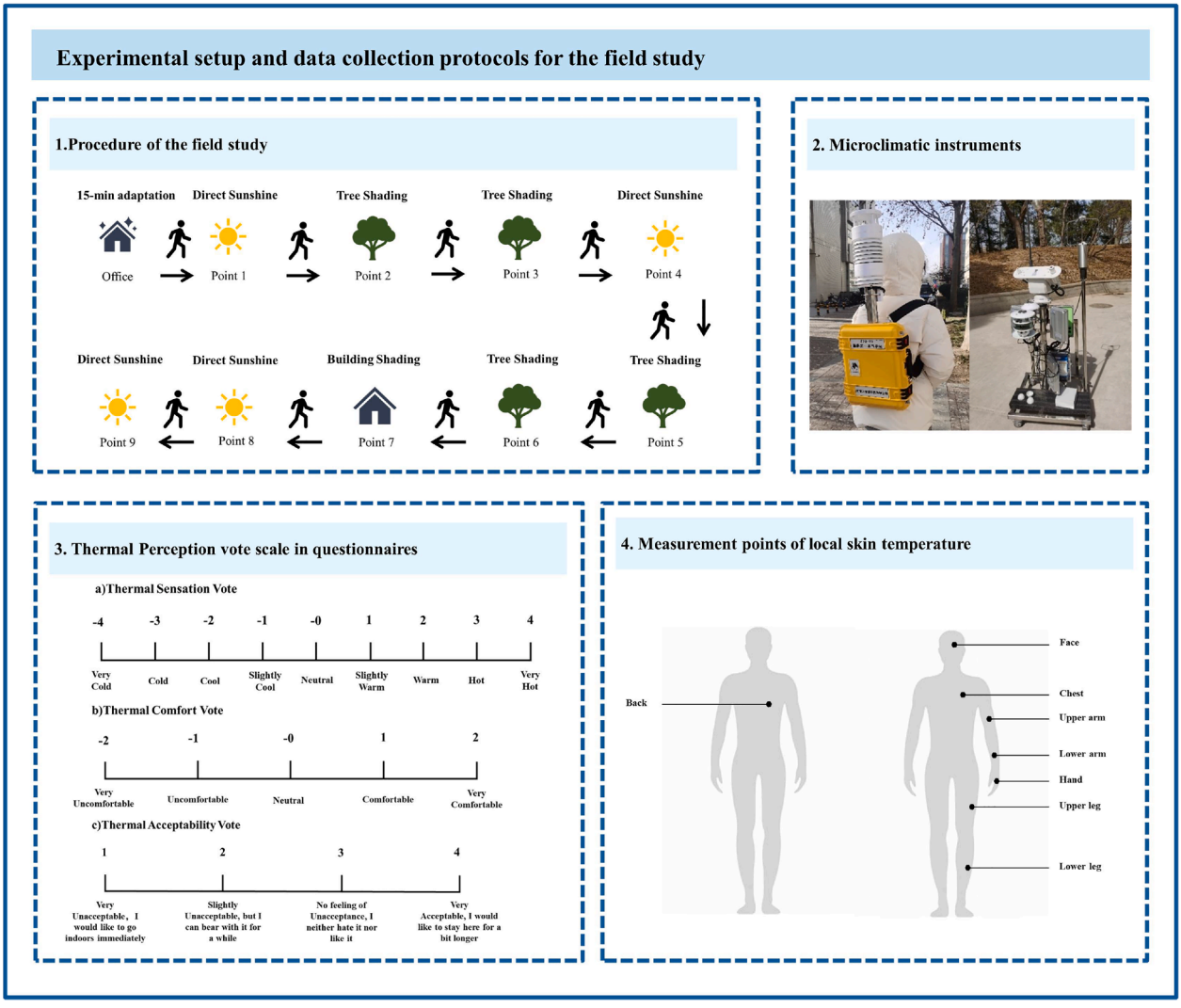

Fig. 2. Experimental setup and data collection protocols for the field study.

2. Method

2.1. Site measurement

The field study was conducted at Tsinghua University, Beijing, from January to August 2021, covering winter, spring, and summer conditions. Initially, a total of 54 volunteers were recruited. After data screening to exclude incomplete responses or sensor errors, 51 valid subjects (19 males and 32 females) were included in the final analysis. Each subject completed one walking trial, and experiments were conducted in pairs, with two subjects walking and stopping synchronously along the route.

Prior to each experiment, a 15-minute preparation period was arranged in a well-ventilated office for acclimation and collecting baseline information (Table S1). During spring and summer, the subjects were primarily dressed in short-sleeved shirts, shorts and skirts. In winter, they wore down jackets and accessorized with scarves, hats, and gloves. Subsequently, subjects walked along a 1.0 km designated route at a controlled speed of 0.9 m/s. The route comprised 9 measurement locations spaced 108 to 219 m apart, covering diverse shading conditions (Fig. 2). The height-to-width ratios (H/W) and proximity to buildings at each location were quantified using Google Earth Pro and are summarized in Table S2. No open water bodies were present along or around the experimental route. At each location, subjects stopped briefly (approx. 30 to 60 s) to complete the thermal perception questionnaires (thermal sensation vote *(TSV),* thermal comfort vote *(TCV),* and thermal acceptability vote *(TAV)*) immediately upon arrival.

During the walk, a backpack-type monitoring system was used to record real-time microclimate parameters (air temperature (T_a), relative humidity (RH), relative wind speed (v), downward short-wave radiation (Q_{sw-d}), and longitude and latitude (Fig. 2). Local skin temperatures were continuously recorded according to the body sites marked in Fig. 2. The technical specifications of all instruments are listed in Table S3. Further experimental details can be found in our previous published study [48].

2.2. Calculation of real-time thermal storage

The human body thermal storage (TS) is influenced by internal heat production resulting from metabolism and external heat exchange with the surrounding environment. This heat exchange occurs through various processes, including radiation, conduction, convection, evaporation, and respiration. Real-time T_a, RH, mean radiant temperature (T_{mrt}), v and $T_{sk,i}$ were obtained from measurements, clothing value (I_{cl}) was determined based on the ASHRAE 55 standards [49], and *Height, Weight, Sex* and *Age* of the subjects were gathered from indoor questionnaires, while skin wettedness (ω) was simulated using the *JOS-3* model. A supplementary sensitivity analysis indicated that a ±20 % variation in ω led to a deviation of only 9.1 % in the final TS calculation, ensuring the robustness of the results. This section presents the calculation method of overall and local thermal storage. For each subject, the real-time TS was derived from experimental measurements and computed every five seconds in Python using the following equations. The simulated TS calculation, however, involves two steps: first, determining the physiological parameters that correspond to the threshold of the thermoneutral zone, and then computing the TS based on those simulated parameters.

2.2.1. Energy balance of the human body with its environment

The calculation of overall (or local) TS was based on the thermal interaction of the human body with its environment. Eq. (1) was used to determine overall or local TS, where i becomes invalid when calculating overall TS, and valid when calculating local TS.

$$TS_{(i)} = (M_{(i)} - W_{(i)} + R_{S(i)}) - (C_{(i)} + R_{L(i)}) - E_{sk(i)} - Q_{res(i)} \quad (1)$$

Where:

$TS_{(i)}$: Rate of overall (local) thermal storage per unit of skin area, W/m^2;

$M_{(i)}$: Rate of overall (local) metabolic heat production, W/m^2;

W_i: Rate of overall (local) mechanical work accomplished, W/m^2, as recommended by the ASHRAE handbook [49], W_i is set as 0 in this study.

$R_{S(i)}$: Rate of overall (local) short-wave radiative heat gain, W/m^2;

$C_{(i)}$: Rate of overall (local) convective heat loss from skin, W/m^2;

$R_{L(i)}$: Rate of overall (local) long-wave radiative heat loss from skin, W/m^2;

$E_{sk(i)}$: Rate of overall (local) evaporative heat loss from skin, W/m^2;

$Q_{res(i)}$: Rate of overall (local) respiratory heat loss, W/m^2.

2.2.2. Mean skin temperature

The local convective and radiative heat exchanges were calculated using the measured

$T_{sk,i}$, while the overall convective and radiative heat exchanges were calculated based on the calculated mean skin temperature, determined by the eight-point method developed by Gagge and Nishi [50] as illustrated in Eq. (2). Specially, T_{head} was measured at the cheek, and $T_{forearm}$ was measured at the lower arm.

$$T_{sk,m} = 0.07T_{head} + 0.175T_{chest} + 0.175T_{back} + 0.07T_{upper\ arm} + 0.07T_{forearm} + 0.05T_{hand} + 0.19T_{thigh} + 0.20T_{leg} \quad (2)$$

Where:

$T_{sk,m}$: Mean skin temperature, °C;

$T_{body\ segment}$: Local skin temperature for each body segment, °C.

2.2.3. Body surface area

The calculation of body surface area (BSA) is essential for calculating both overall and local TSs, as it is influenced by the heat gain or loss per unit surface area. In this study, the overall body surface area (BSA_{all}) of each subject was calculated following the DuBois method [51] using Eq. (3). The local body surface area (BSA_i) was calculated based on the ratio of body surface area to standard body surface area (BSA_{ra}) and body surface area of the standard body (BSA_{st}) using Eq. (4). The standard body surface area was defined as 1.87 m^2 for a subject who is 1.73 m tall and weighs 70 kg. BSA_{ra} can be calculated using Eq. (5) [52], and BSA_{st} is shown in Table S4.

$$BSA_{all} = 0.202 \cdot Weight^{0.425} \cdot Height^{0.725} \quad (3)$$

$$BSA_i = BSA_{ra} \cdot BSA_{st} \quad (4)$$

$$BSA_{ra} = BSA_{all}/1.87 \quad (5)$$

Where:

BSA_{all}: Overall body surface area, m^2;

$Weight$: Human body weight, kg;

$Height$: Human body height, m;

BSA_i: Local body surface area, m^2;

BSA_{ra}: Ratio of body surface area to standard body surface area;

BSA_{st}: Body surface area of the standard body, m^2.

2.2.4. Rate of overall (local) metabolic heat production

Heat production within the human body can be divided into four components: basal metabolic rate in the thermally neutral state, changes in local basal metabolism caused by thermal state change, external work, and shivering. In this study, changes in local basal metabolism caused by thermal state change and shivering were not considered. Statistically, supportive research has recorded only an 8 % change in oxygen uptake for subjects performing submaximal exercise when the ambient temperature increased from 21°C to 49°C [53,54], and this

change would be even less under sedentary conditions. Therefore, the amount of increase in basal metabolism can be considered negligible with the change of thermal state in the current experiments.

The rates of overall (or local) metabolic heat production ($M_{(i)}$) in this study were calculated by Eq. (6), represented as the sum of heat production by overall (or local) basal metabolism and external work per unit of skin area. Eqs. (6–14) relate to the calculation of overall (or local) M, where i becomes invalid when calculating overall M, and valid when calculating local M. The calculation method of overall heat production by basal metabolism (M_{base}) refers to the Harris–Benedict model shown in Eqs. (7,8), which considers physiological difference in gender, height, weight and age [55,56]. The basal metabolic heat production of each body segment ($M_{base,i}$) can be obtained by Eq. (9), adding the heat produced by each segment's basal metabolism from core ($M_{base_{cr,i}}$), muscle ($M_{base_{ms,i}}$), fat ($M_{base_{fat,i}}$) and skin ($M_{base_{sk,i}}$). These four terms were determined by Eqs. (10–13) respectively.

Additionally, the metabolic energy accounted for by external work for the whole body (M_{work}) was determined by Eq. (14) [57], while the corresponding energy associated with external work at the local body segment ($M_{work,i}$) was calculated by Eq. (15), following the *JOS-3* model [52]. The physical activity ratio (*PAR*) was selected as 2.0 according to the ASHRAE 55 standard [49], and the distribution coefficients of heat production by basal metabolism and work for different anatomical segments ($f_{base_{cr},i}$, $f_{base_{ms,i}}$,$f_{base_{fat,i}}$, $f_{base_{sk,i}}$, $f_{work,i}$) shown in Table S5 were cited from the *JOS-3* model [52].

$$M_{(i)} = (M_{base(i)} + M_{work(i)})/BSA_{(i)} \tag{6}$$

$$Male:\ M_{base} = \begin{pmatrix} 88.362 + 500.3\cdot Height + \\ 13.397\cdot Weight - 5.677\cdot Age \end{pmatrix}\cdot 0.048 \tag{7}$$

$$Female:\ M_{base} = \begin{pmatrix} 447.593 + 479.9\cdot Height + \\ 9.247\cdot Weight - 4.330\cdot Age \end{pmatrix}\cdot 0.048 \tag{8}$$

$$M_{base(i)} = M_{base\_cr(i)} + M_{base\_ms(i)} + M_{base\_fat(i)} + M_{base\_sk(i)} \tag{9}$$

$$M_{base_{cr}(i)} = M_{base}\cdot f_{base_{cr}(i)} \tag{10}$$

$$M_{base_{ms}(i)} = M_{base}\cdot f_{base_{ms}(i)} \tag{11}$$

$$M_{base_{fat}(i)} = M_{base}\cdot f_{base_{fat}(i)} \tag{12}$$

$$M_{base_{sk}(i)} = M_{base}\cdot f_{base_{sk}(i)} \tag{13}$$

$$M_{work(i)} = f_{work(i)}\cdot(PAR - 1)\cdot M_{base} \tag{14}$$

Where:

$M_{(i)}$: Rate of overall (local) metabolic heat production, W/m^2;

$M_{base(i)}$: Heat production by overall (local) basal metabolism, W;

$M_{work(i)}$: Heat production by overall (local) external work, W;

Height: Human body height, m;

Weight: Human body weight, kg;

$M_{base\_cr(i)}$, $M_{base_{ms}(i)}$, $M_{base_{fat}(i)}$, $M_{base_{sk}(i)}$: Heat production by basal metabolism from core, muscle, fat and skin of whole body (each body segment), W;

$M_{work(i)}$: Heat production by external work in whole (local) body, W;

$f_{base_{cr}(i)}$,$f_{base_{ms}(i)}$,$f_{base_{fat}(i)}$,$f_{base_{sk}(i)}$,$f_{work(i)}$: Distribution coefficient of heat production by basal metabolism and work for whole body (different segments).

2.2.5. Mean radiant temperature

Due to the simplification of radiation measurements using a pair of upward- and downward-facing hemisphere sensors, an simplified method was employed to calculate T_{mrt}, assuming that the human body is approximated as an unshaded plane, and the solid angles of the surface and the sky were set as 0.5 [58], Eq. (15) was used to calculate T_{mrt} [48].

$$T_{mrt} = \sqrt[4]{\frac{f_a\left(a_k(Q_{sw-u} + Q_{sw-d}) + \varepsilon_p(Q_{lw-u} + Q_{lw-d})\right)}{\varepsilon_p\sigma}} - 273.15 \tag{15}$$

where:

T_{mrt}: Mean radiant temperature, °C;

f_a: Solid angle factor for the upward and downward hemispheres ($f_a = 0.5$);

a_k: Absorption coefficient for short-wave radiation (standard value 0.7);

ε_p: Emissivity of the clothed human body for long-wave radiation (standard value 0.97);

Q_{sw-u}: Upward short-wave radiation, W/m^2;

Q_{sw-d}: Downward short-wave radiation, W/m^2;

Q_{lw-u}: Upward long-wave radiation, W/m^2;

Q_{lw-d}: Downward long-wave radiation, W/m^2;

σ: Stefan–Boltzmann constant ($\sigma = 5.67 \times 10^{-8}\ W/(m^2K^4)$).

2.2.6. Rate of overall (local) short-wave radiative heat gain

The amount of direct ($R_{s_{dir}}$) and diffuse $\left(R_{s_{dif}}\right)$ solar radiation received by an individual depends on the direct ($f_{p_{dir}}$) and diffuse ($f_{p_{dif}}$) projected area factors, the geometry-related and direction-dependent radiation parameters of the human body, respectively. Therefore, the calculation of the heat gain from short-wave solar radiation is presented in Eq. (16–18) [59]. The intensity of direct short-wave solar radiation (Q_{dir}) was measured during the experiment, and the intensity of diffuse short-wave solar radiation $\left(Q_{dif}\right)$ could be computed from Eq. (19) [60]. $R_{s_{dir}}$ was distributed to each body segment based on $f_{p_{dir}}$, which was influenced by the relative azimuth angle (α) and altitude angle (β) (shown in Fig. 3) of the human body to the sun. These two numerical values were calculated based on latitude, longitude and walking direction. The local direct projected area factor was considered as a function of these two angles calculated following the mathematical expression in Eq. (20-21), and the coefficients were selected from Kubaha et al [61]. $R_{s_{dif}}$ was also distributed to each body segment based on $f_{p_{dif}}$, which was decided by the ground albedo (ρ). The local diffuse projected area factor was calculated as Eq. (22), and the relative coefficient was cited from Kubaha et al [61]. The ground albedo was the ratio of upward and

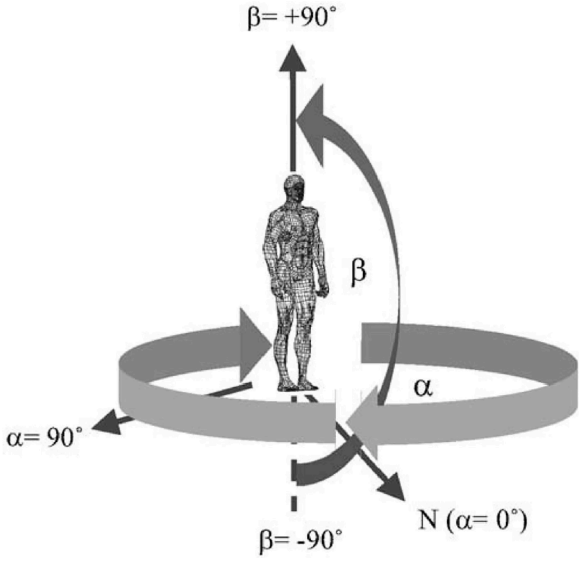

Fig. 3. Geometric notations referring to the determination of the projected area factor of a pedestrian [61].

downward short-wave radiation, and is presented in Eq. (23). Specifically, the absorption rate of all subjects' clothing was assumed to be constant.

$$R_{S(i)} = R_{s_{dir}(i)} + R_{s_{dif}(i)} \tag{16}$$

$$R_{S_{dir}(i)} = f_{p_{dir}(i)} \cdot a_k \cdot Q_{dir} \tag{17}$$

$$R_{S_{dif}(i)} = f_{p_{dif}(i)} \cdot a_k \cdot Q_{dif} \tag{18}$$

$$Q_{dif} = (Q_{sw-u} + Q_{sw-d}) - Q_{dir} \cdot \sin\beta \tag{19}$$

$$f_{p_{dir}(i)} = [A_{(i)} \cos\ (C_{1(i)}\ \alpha + C_{0(i)}) + B_{(i)}] \cdot S_{(i)} \tag{20}$$

$$S_{(i)} = 1 + \frac{\tanh(D_{1(i)}\ \alpha + D_{0(i)})}{2} + \frac{\tanh(E_{1(i)}\ \alpha + E_{0(i)})}{2} \tag{21}$$

$$f_{p_{dif}(i)} = g_{1(i)}\ \rho + g_{0(i)} \tag{22}$$

$$\rho = Q_{sw-u}\ /\ Q_{sw-d} \tag{23}$$

Where:

$R_{S(i)}$: Rate of short-wave radiation absorbed by body surface of whole body (each body segment), W/m^2;

$R_{s_{dir}(i)}$: Rate of direct short-wave radiation absorbed by body surface of whole body (each body segment), W/m^2;

$R_{s_{dif}(i)}$: Rate of diffuse short-wave radiation absorbed by body surface of whole body (each body segment), W/m^2;

$f_{p_{dir}(i)}$: Projected area factor of whole body (each body segment) exposed to the direct short-wave radiation;

$f_{p_{dif}(i)}$: Projected area factor of whole body (each body segment) exposed to the diffuse short-wave radiation.

a_k: Short-wave absorptivity of the body surface;

Q_{dir}: The intensity of direct short-wave solar radiation,$W\ /m^2$;

Q_{dif}: The intensity of diffuse short-wave solar radiation,$W\ /m^2$;

α: Relative azimuth angle, *rad*;

β: Altitude angle, *rad*;

$A_{(i)}, B_{(i)}, C_{1(i)}, C_{0(i)}$: Regression coefficients selected for projected area factor of whole body (each body segment) exposed to the direct short-wave radiation;

$S_{(i)}$: The shading function for projected area factor of whole body (each body segment) exposed to the direct short-wave radiation;

$D_{1(i)}, D_{0(i)}, E_{1(i)}, E_{0(i)}$: Regression coefficients selected for the shading function;

$g_{1(i)}, g_{0(i)}$: Regression coefficients selected for projected area factor of whole body (each body segment) exposed to the diffuse short-wave radiation;

ρ: Ground albedo.

2.2.7. Rate of overall (local) convective and long-wave radiative heat loss from skin

The overall (local) convection and long-wave radiation heat loss were calculated by Eqs. (24–30) [52,62]. In these equations, *i* is invalid for overall heat loss but valid for local heat loss. The experiment only measured microclimate conditions at pedestrian height, so it was assumed that each body segment was exposed to the same external thermal conditions. To calculate subject's $I_{cl,i}$, the relative coefficients $f_{0,i}$ and $f_{1,i}$ were cited from Tang et al [63] and Lin et al [64].

$$C_{(i)} = f_{cl(i)} \cdot h_{c(i)} \cdot (T_{cl(i)} - T_a) \tag{24}$$

$$R_{L(i)} = f_{cl(i)} \cdot h_{r(i)} \cdot (T_{cl(i)} - T_{sr}) \tag{25}$$

$$T_{cl(i)} = \frac{T_{sk(i)} + R_{cl} f_{cl(i)}\ h_{c(i)}\ T_a + R_{cl} f_{cl(i)}\ h_{r(i)}\ T_{sr}}{1 + f_{cl(i)} \cdot R_{cl} f_{cl(i)}\ h_{c(i)}\ + R_{cl} f_{cl(i)}\ h_{r(i)}} \tag{26}$$

$$R_{cl(i)} = 0.155 \cdot I_{cl(i)} \tag{27}$$

$$f_{cl(i)} = 1.00 + 0.3 I_{cl(i)} \tag{28}$$

$$I_{cl,i} = f_{0,i} + f_{1,i} \cdot I_{cl} \tag{29}$$

$$T_{sr} = \sqrt[4]{\frac{f_a \varepsilon_p (Q_{lw-u} + Q_{lw-d})}{\varepsilon_p \sigma}} - 273.15 \tag{30}$$

Where:

$f_{cl(i)}$: Overall (local) clothing area factor that accounts for the increased area due to clothing;

$T_{cl(i)}$: Overall (local) clothing surface temperature, °C;

$h_{c(i)}$: Overall (local) convective heat transfer coefficient, $W/(m^2 \cdot K)$;

$h_{r(i)}$: Overall (local) long-wave radiative heat transfer coefficient, $W/(m^2 \cdot K)$;

T_a: The ambient air temperature, °C;

T_{sr}: The surface temperature of the surroundings, °C;

$T_{sk(i)}$: Overall (local) skin surface temperature, °C;

R_{cl}: Overall (local) thermal resistance of clothing, $(m^2 \cdot K)/W$

$I_{cl(i)}$: Overall (local) thermal resistance of clothing, *clo*;

$f_{0,i}, f_{1,i}$: Regression coefficients selected for thermal resistance of clothing at each body segment.

Convective heat transfer coefficients for different segments were calculated using Yu et al.'s method [65], which was related to both v and turbulence intensity (*TI*), to account for the naturally higher turbulence intensity levels outdoors (as Eqs. (31,32)). The constants A, B, and n shown in Table S6 are segment-specific constants used in the calculation.

$$h_c = A v^n \times \left(1 + B\ TI \times v^{0.5}\right) \tag{31}$$

$$TI = \left(\frac{std_v}{mean_v}\right) \cdot 100\% \tag{32}$$

Specifically, when the v is less than 0.1 m/s, the subjects can be considered as standing in still air. In this case, the convective heat transfer coefficients were referred to de Dear et al. [66] (shown in Table S7). The radiative heat transfer coefficients were obtained from the manikin experiments conducted by Yu et al. [65] and are listed in Table S8.

2.2.8. Rate of overall (local) evaporative and respiratory heat loss

The overall (local) evaporative heat loss at the skin surface of each body segment ($E_{(i)}$) was quantified by Eqs. (33,34) [52]. In these equations, *i* is invalid for whole body evaporative heat loss, but valid for local evaporative heat loss. The $\omega_{(i)}$ used in this study was simulated using the *JOS-3* model [52] due to the lack of measuring equipment during the experiment. These data were simulated by using measured environmental parameters, I_{cl}, and personal characteristics of the subjects, metabolic rates, posture, and other relevant factors as input, with outputs generated every 5 s throughout the simulation of the actual field experiment in order to maintain consistency.

$$E_{sk(i)} = \omega_{(i)} \cdot h_{et(i)} \cdot (p_{sk,s(i)} - p_a) \tag{33}$$

$$\frac{1}{h_{e(i)}} = \frac{0.155 \cdot I_{cl(i)}}{L_R \cdot i_{cl(i)}} + \frac{1}{f_{cl(i)} \cdot L_R \cdot h_{c(i)}} \tag{34}$$

Where:

$\omega_{(i)}$: Overall (local) skin wettedness;

$h_{et(i)}$: Overall (local) evaporative heat transfer coefficient, $W/(m^2 \cdot K)$;

$p_{sk,s(i)}$: Overall (local) saturated water vapor pressure at the skin, kPa;

p_a: Water vapor pressure in ambient air, kPa;

L_R: The Lewis constant ($L_R = 16.5\ K/kPa$).

The respiratory heat loss primarily occurs in the head, neck, and

chest, with respective weightings of 45%, 25%, and 30%. The calculation of respiratory heat loss (Q_{res}) is expressed in Eq (35).

$$Q_{res} = [0.0014 \cdot (34 - T_a) + 0.0173 \cdot (5.87 - p_a)] \cdot M \quad (35)$$

2.3. Quantifying thermal alliesthesia zones based on thermal storage

The framework proposed by Parkinson and de Dear [33] presented in Fig. 4 outlines the potential of alliesthesia and corresponding thermal perceptions under different thermal physiological states. The boundary between the metabolic regulatory zone and the thermoneutral zone is identified by the onset of active shivering, while the boundary between the sudomotor regulatory zone and the thermoneutral zone is identified by the onset of active sweating. Although this framework provides a clear theoretical definition, further data from daily activities are needed to establish its practical applicability. In this section, thermal storage data are used to serve this purpose.

Due to limitations of field-based research methods, capturing the precise instantaneous physiological state of a subject at the exact onset of sweating or shivering is challenging. However, for a given individual with specific anthropometrics, these onset thresholds are intrinsic and remain constant. Therefore, by varying the simulated thermal conditions, the corresponding physiological state at each onset setpoint can be estimated. The reliability of the *JOS-3* model in capturing dynamic thermoregulatory responses (e.g., skin temperature RMSE < 0.6°C and evaporative loss error < 7 g) has been rigorously validated in similar transient protocols [67]. The control equations of shivering and sweating inside the *JOS-3* model are provided in Eq. (36-42), which follow those originally proposed by for the Stolwijk model [68] (detailed descriptions are provided in Section S2).

$$\mathrm{Err}_{j(i)} = \mathrm{T}_{j(i)} - \mathrm{T}_{setpt,j(i)} \quad (36)$$

$$SWEAT = 371.2 \cdot \mathrm{Err}_{cr(0)} + 33.64 \cdot (\mathrm{WARMS} - \mathrm{COLDS}) \quad (37)$$

$$SHIV = 24.36 \cdot \mathrm{COLD}_{cr(0)} \cdot \mathrm{COLDS} \quad (38)$$

$$\mathrm{WARM}_{(i)} = \begin{cases} 0 \ (\mathrm{Err}_{sk(i)} \le 0) \\ \mathrm{Err}_{sk(i)} \ (\mathrm{Err}_{sk(i)} > 0) \end{cases} \quad (39)$$

$$\mathrm{COLD}_{(i)} = \begin{cases} 0 \ (\mathrm{Err}_{sk(i)} > 0) \\ -\mathrm{Err}_{sk(i)} \ (\mathrm{Err}_{sk(i)} \le 0) \end{cases} \quad (40)$$

$$WARMS = \sum_{i=0}^{n} \mathrm{SKINR}_{(i)} \cdot \mathrm{WARM}_{(i)} \quad (41)$$

$$COLDS = \sum_{i=0}^{n} \mathrm{SKINR}_{(i)} \cdot \mathrm{COLD}_{(i)} \quad (42)$$

Where:

$\mathrm{Err}_{j(i)}$: error signal for human body, °C; j: body tissue type (core, muscle, fat, skin); i: body anatomical segment;

$\mathrm{T}_{j(i)}$: Instantaneous temperature of body, °C;

$\mathrm{T}_{setpt,j(i)}$: setpoint temperature of the body, °C;

SWEAT: sweating signal, W;

SHIV: shivering signal, W;

WARMS: integrated error signal in the warm receptor, °C;

COLDS: integrated error signal of cold receptor, °C.

According to the control equations of the *JOS-3* model, the triggering of sweating and shivering depends solely on the instantaneous $T_{sk,i}$ and the core temperature of the head, independent of the pathway by which these critical values are reached. In other words, the thermal state corresponding to the boundaries of the thermoneutral zone remains invariant. Therefore, to simplify the simulation process, the input conditions for each subject were set to the average climatic parameters of the corresponding season, with only T_a and individual participant's anthropometrics being varied. The simulation duration was set to 5000 s to ensure sufficient time for subjects to reach a state of either sweating or shivering. The moment when the *JOS-3* output variable *Esweat* (evaporative heat loss at the skin due to sweating alone) becomes greater than zero was identified as the onset of sweating, while the moment when the output variable *Mshiv* (heat production by shivering) becomes larger than zero was regarded as the onset of shivering. The corresponding values of $T_{sk,m}$, ω, and T_a at these times were selected to calculate the *TS* value based on the method in Section 2.2, thereby determining the boundary of the thermoneutral zone for each subject. The Overview steps of quantifying thermal alliesthesial zones from thermal storage data is shown in Fig. 5.

2.4. Data analysis

To ensure data quality, measurements were preprocessed to remove outliers (~5.16 %, interpolated) and noise using a 30-point sliding window-based three-standard deviation method and a Savitzky-Golay filter [69] (window=5, order=2), respectively. The associations between changes in *TS* and *TCV* were explored using regression methods. R^2 was used to evaluate the quality of fit in regression analysis. A Pearson correlation analysis was employed to examine the relationship between *TS* during the 105 s preceding the questionnaire submission and *TCV* at the time of questionnaire submission, and the *p-values* were set at 0.01. Furthermore, feature importance was assessed using a Gradient Boosting [70] classifier to analyze the relationship between the local *TS* and the overall *TCV* of subjects. Also, to avoid ambiguity, the specific definitions, calculation windows, and analytical roles of the different *TS* metrics are consolidated in Table S9.

3. Results and discussion

3.1. Thermal conditions

3.1.1. Microclimate conditions

The overview of T_a and *RH* during the experiment across seasons is presented in Table 1. The average T_a recorded in the winter, spring and summer is -2.2 °C, 22.8 °*C* and 27.8 °*C*, respectively. In winter, the variation in T_a is notably high, with a standard deviation of 5.1 °C and a difference of 15.5 °C between the minimum and maximum values. The variation of the summer experiment is greater than in the spring, with a range of 9.5 °C in summer compared to 6.5 °*C* in spring. This variation difference has also been observed during each experiment section, with the standard deviation of T_a recorded during summer sections larger

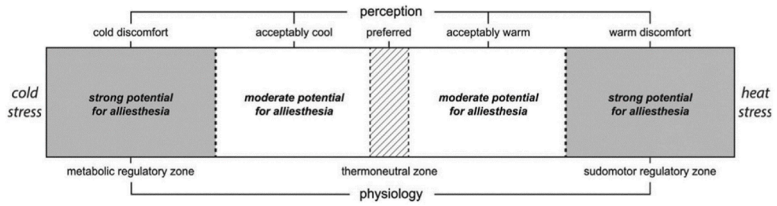

Fig. 4. A conceptual model that pairs zones of physiological thermoregulation with thermal perception adjectives [33].

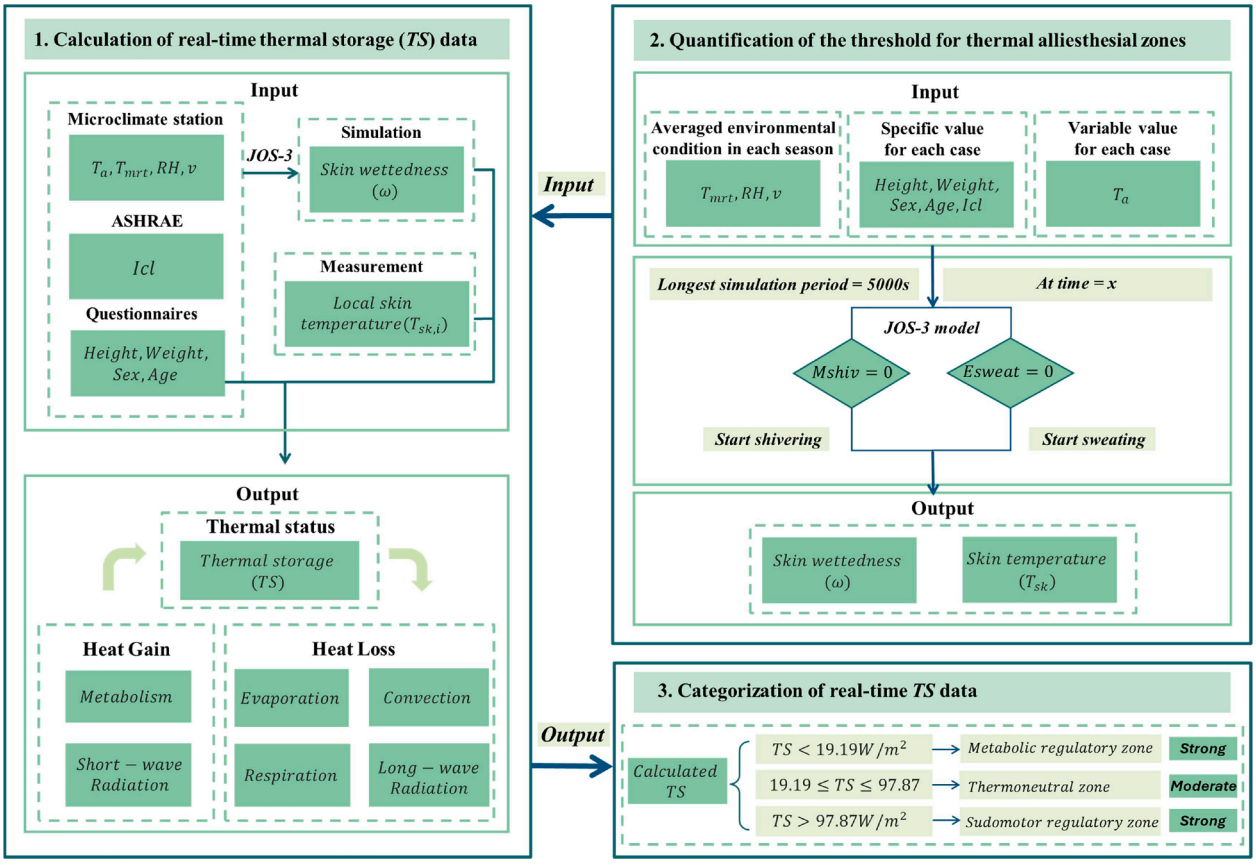

Fig. 5. Overview of quantifying thermal alliesthesial zones from thermal storage data.

Table 1
Brief information of T_a and *RH* during experiments across different seasons.

	Winter		Spring		Summer	
	T_a (°C)	*RH* (%)	T_a (°C)	*RH* (%)	T_a (°C)	*RH* (%)
Average	-2.2	17.1	22.8	26.4	27.8	47.6
Standard deviation	5.1	2.9	1.8	14.4	2.4	11.9
Maximum	4.5	21.4	26.8	50.9	32.5	78.8
Minimum	-11.0	11.3	20.3	6.7	23.0	26.3

than during spring sections. The *RH* level in summer Beijing was higher than in spring, with the average *RH* in summer being 47.6 % and in spring being 26.4 %. While winter is extremely dry, with a very low *RH* value of only 17.1 %.

Fig. 6 plots time-series data on typical dates to illustrate the variation of v and T_{mrt} along the experimental route. The v conditions differed markedly between the three seasons, with winter data showing higher average and standard deviation values (1.7 m/s and 1.4 m/s). Compared to winter, the summer and spring data are generally more stable, with similar average values and identical standard deviations (1.2 m/s and 0.8 m/s vs 1.1 m/s and 0.8 m/s, respectively). The change in prevailing wind direction causes a noticeable spatial difference of wind conditions between the three seasons. For instance, the maximum v in summer occurred at *P3_Tree*, while in spring and winter, the maximum values were recorded at the *P5_Tree - P6_Tree* section.

The T_{mrt} value fluctuated dramatically in the whole experiment sections due to changes in solar azimuth and altitude across three seasons. Its levels in spring and summer were significantly greater, presenting a sharp contrast to the much lower values recorded in winter. As subjects walked from *P1_Sun* to *P9_Sun* along the pre-designed experimental route, they encountered various transitions in thermal environments, resulting in different levels of heating or cooling across their body segments. Natural environments can thus induce thermal alliesthesia and affect thermal comfort levels.

3.1.2. Human body thermal state

A summary of *TS* distribution and the relationship between overall *TS* and subjective thermal perceptions, including *TSV, TCV*, and *TAV*, is provided in this section. The overall *TS* was calculated by taking the average data from the 15 s before and after the point in time when the subjects started the survey at each survey point.

Fig. 7 shows the distribution of overall *TS* and time-series data representing changes in various avenues of body heat gain and loss during the winter, spring and summer experiments. The average overall *TS* values range from -5.8 to 153.8 W/m^2 in winter, from 43.7 to 155.3 W/m^2 in spring, and from 51.0 to 157.2 W/m^2 in summer (as shown in Fig. 7 (left)). The maximum overall *TS* for all seasons occurs at *P1_Sun*, and the minimum occurs at *P7_Building*. Short-wave radiation heat gain is the primary factor driving variations in overall *TS* along the experimental route in all seasons. Convective and long-wave radiative heat losses are the two most significant factors, with larger variation observed in winter due to stronger v than summer and spring (as shown in Fig. 7 (right)).

Fig. 8 shows the distribution of *TS* across different *TSVs*. Overall, *TS* increases with higher *TSV* levels; however, the rate of increase varies among adjacent sensation levels. Based on the mean *TS* values for each *TSV* category, the required increase in *TS* from "0" to "+1" is 28.9 W/m^2, which is substantially larger than for other positive *TSV* increments, which are generally within 20 W/m^2. On the negative side, the changes from "-1" to "-2" and from "-3" to "-4" are much greater, each reaching approximately 50 W/m^2.

The average overall *TS* values decrease as comfort and acceptable levels increase, but the decreases are relatively small for each scale

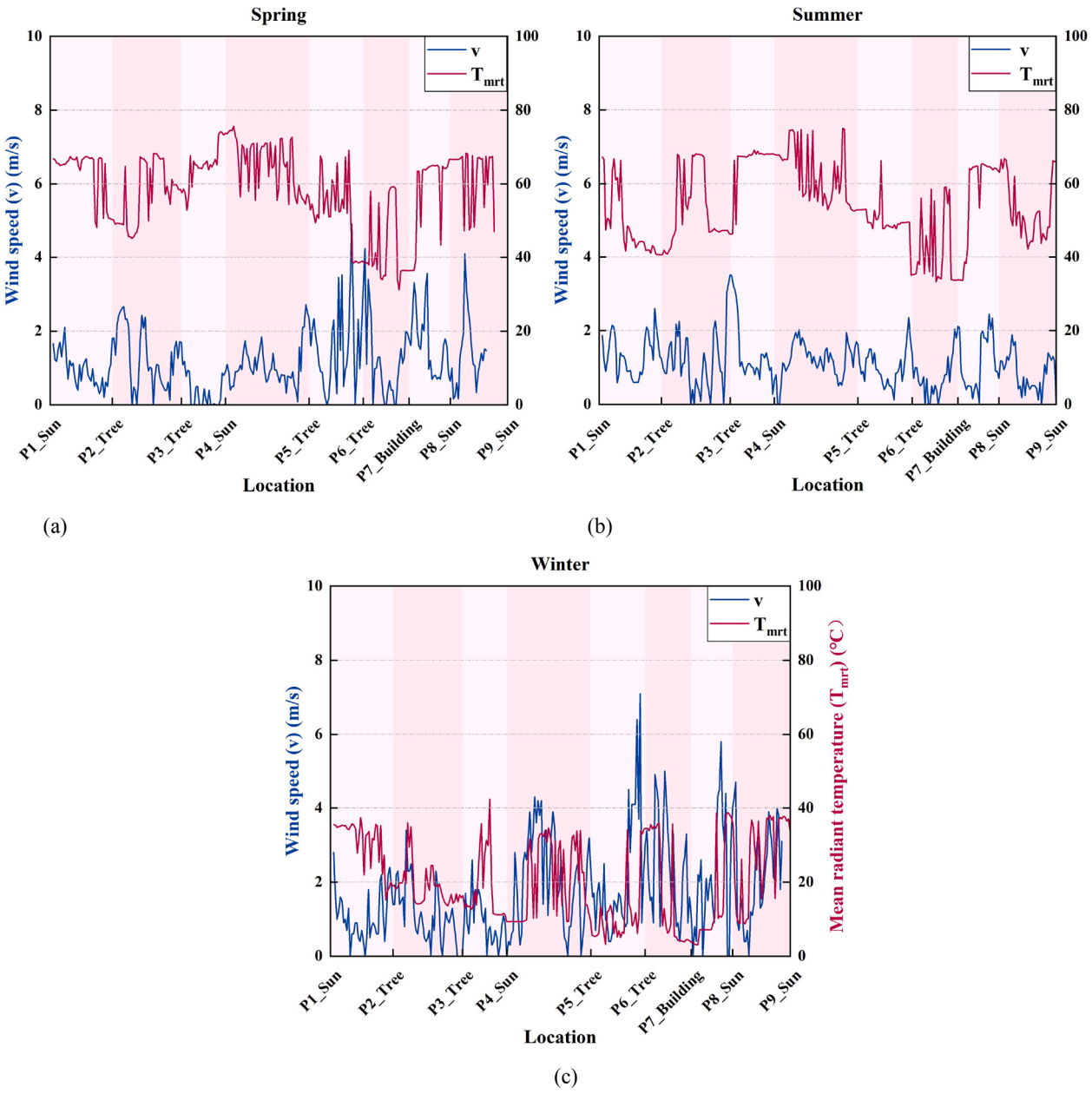

Fig. 6. Example relative wind speed and mean radiant temperature observations along the walking route in different seasons; (a) Spring; (b) Summer; (c) Winter.

(shown in Fig. 8 (b, c)). When analyzing the distribution of *TS* on different *TCV* and *TAV* scales, it is evident that the distribution of *TS* for *TCV* on the negative side is more dispersed than for *TCV* on the positive side. A similar pattern is also observed in the distribution of *TS* for different *TAV* scales. It appears that merely including the *TS* at the time the subjects arrive at the survey points does not suffice to quantify thermal comfort or thermal acceptability levels when the subjects feel thermally uncomfortable or unacceptable.

The changes in thermal storage (*dTS*) along with the changes in *TSV* (*dTSV*), *TCV* (*dTCV*) and *TAV* (*dTAV*) between each survey points are calculated following Eqs. (43–45). TS_{p_n} represents the thermal storage at the current survey point, and $TS_{p_{n+1}}$ represents the thermal storage at the next survey point, the same definition also applies to *TSV, TCV*, and *TAV*.

$$dTS = TS_{p_{n+1}} - TS_{p_n} \tag{43}$$

$$dTSV = TSV_{p_{n+1}} - TSV_{p_n} \tag{44}$$

$$dTCV = TCV_{p_{n+1}} - TCV_{p_n} \tag{45}$$

The distributions of *dTS* at different *dTSV, dTCV*, and *dTAV* scales are presented in a violin plot in Fig. 9. The recorded change in *TSV* ranged from "-4" to "+4", *TCV* varied on 2 scales, while *TAV* varied on 3 scales. Although data points near the extreme ends of the scales were limited, the observed variation in thermal perceptions along the route was noteworthy and exceeded our expectations. According to Fig. 9 (a), the average *dTS* required for a 1-scale *dTSV* is 22.6 W/m^2 for positive changes and 32.9 W/m^2 for negative changes. An increase in *dTSV* by 2-scale requires a similar change in *dTS*, which is 18.5 W/m^2, while a decrease requires 35.6 W/m^2. A 3-scale change in *dTSV* necessitates a much larger *dTS* variation at both positive and negative sides, reaching over 50 W/m^2.

Since the analysis in this study is predominantly based on data collected during spring and summer, with a significantly smaller sample size from winter, both *dTCV* and *dTAV* showed a negative relationship with *dTS*. It is obvious that the *dTCV* and *dTS* follow a logarithmic

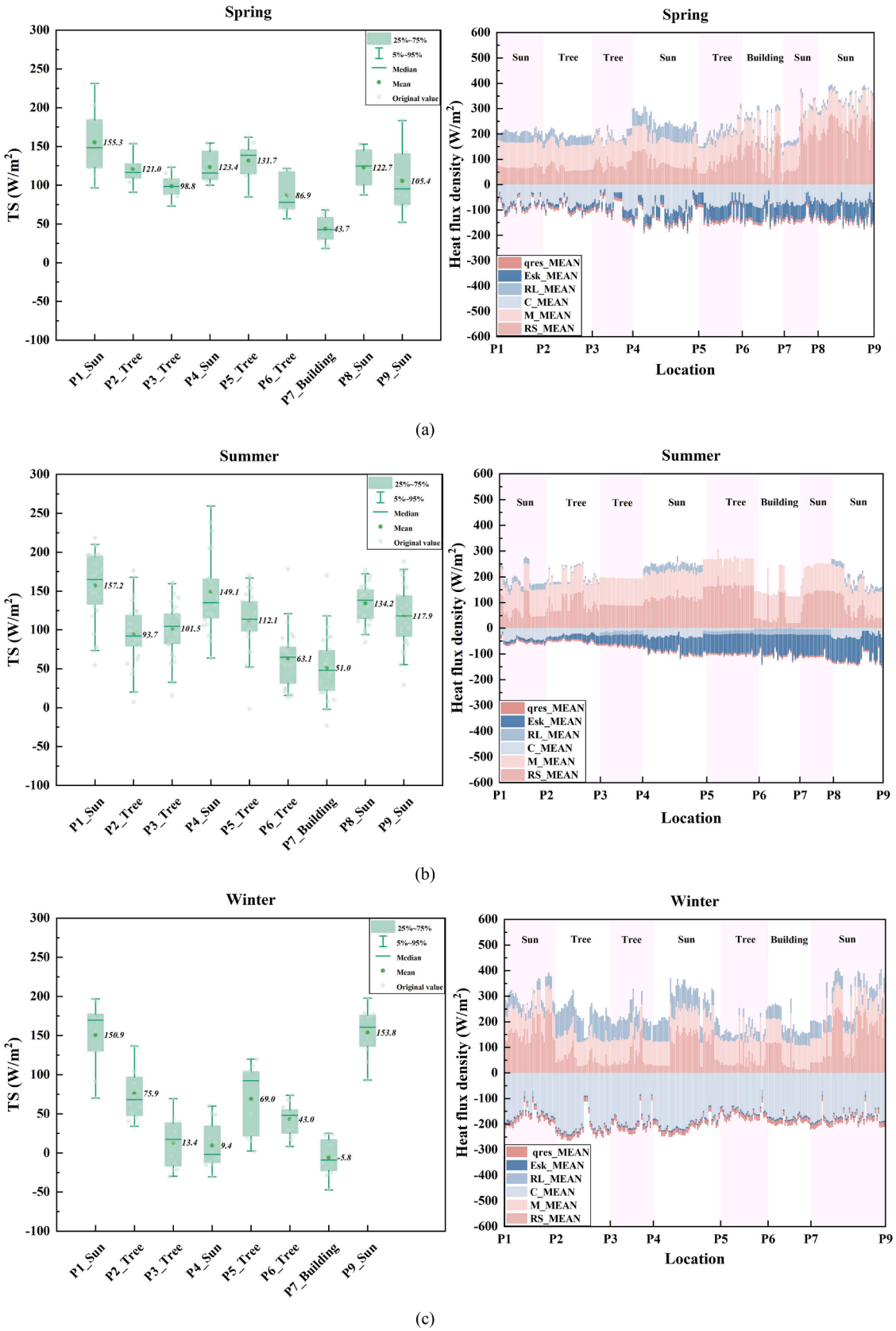

Fig. 7. Summary of *TS* distribution: *TS* box plot at each survey point (left) and Time-series data sample of changes in varioues forms of heat gain and heat loss (right); (a) Spring; (b) Summer; (c) Winter.

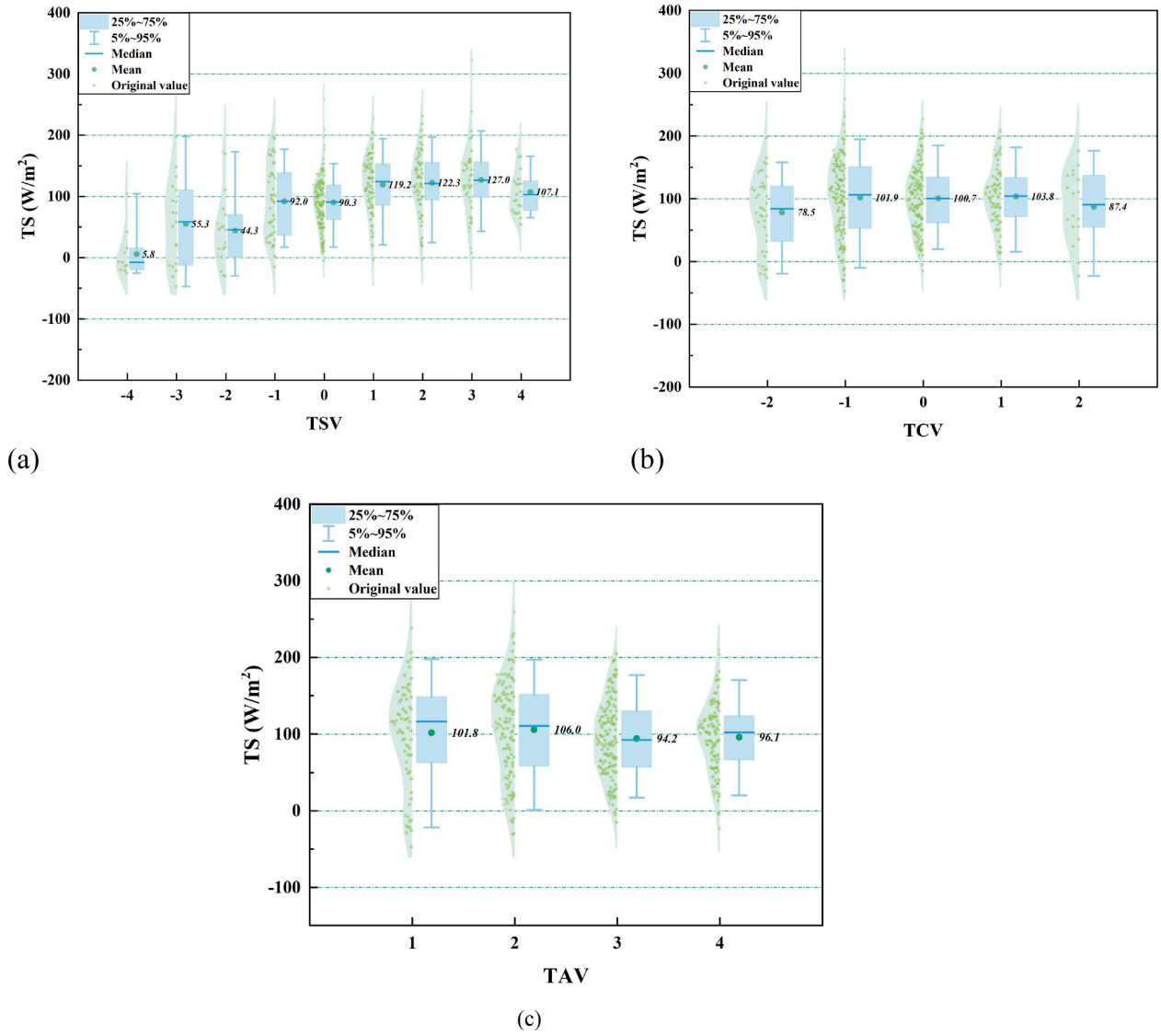

Fig. 8. Distribution of *TS* under different thermal evaluations; (a) *TSV*; (b) *TCV* (c) *TAV*.

function relationship. When *dTCV* ranges from "-1″ to "1", for 1-scale *dTCV*, the average *dTS* is almost symmetrical, with a 17.3 W/m^2 for positive change and 10.8 W/m^2 for negative change. However, for a 2-scale *dTCV*, the response of the average *dTS* is asymmetric, being stronger for negative changes (45.7 W/m^2) than for positive ones (22.37 W/m^2). As for *dTAV* and *dTS*, they are following a linear relathionship. When *dTAV* is around 0, the difference in change of average *dTS* required for a change between adjacent *dTAV* levels is not significant. However, when *dTAV* is at the two extremes, it becomes very pronounced.

3.2. Quantified result of thermal alliesthesial framework based on thermal storage

3.2.1. Simulation results of threshold for thermoneutral zone

Following the simulation methodology described in Section 2.3, the thresholds for the onset of sweating and shivering were calculated for each subject across different seasons. These distributions are presented in Fig. 10, with the specific simulation outputs detailed in Table 2. According to the simulation results, the average *C*, R_L and E_{sk} of subjects in summer are all higher than those in spring. This difference is primarily driven by the variation in I_{cl} between the two seasons. The smaller average I_{cl} in summer (0.42 clo), compared with spring (0.67 clo), increased the temperature gradient between the clothing surface and the ambient environment, resulting in greater overall heat loss. Additionally, the slightly higher average *v* in summer led to a higher h_{et}, which contributed to the greater E_{sk}. In contrast, the average *M*, R_S and Q_{res} remain relatively consistent between these two seasons. Compared with spring, subjects experienced approximately one hour of heat exposure through outdoor walking in summer. This prior exposure likely contributed to the earlier onset of sweating [71]. Similarly, cold acclimatization from the spring environment reduced the rate of heat loss, thereby delaying the onset of shivering. As a result, the mean threshold for subjects in summer shifts toward lower values compared to spring. Specifically, the values were 17.5 W/m^2 on the shivering side and 15.6 W/m^2 on the sweating side. The final thresholds for the thermoneutral zone were determined as the mean values of all subject thresholds from spring and summer, which are 8.05 W/m² and 93.23 W/m², respectively. Ultimately, this framework was categorized into three distinct zones based on the *TS* value, as illustrated in Fig. 11. When $TS \leq 8.05$ W/m² or $TS \geq 93.23$ W/m², there is a strong potential for triggering positive alliesthesia. In contrast, when *TS* falls within the range of 8.05 to 93.23 W/m², only a moderate potential exists for triggering positive alliesthesia.

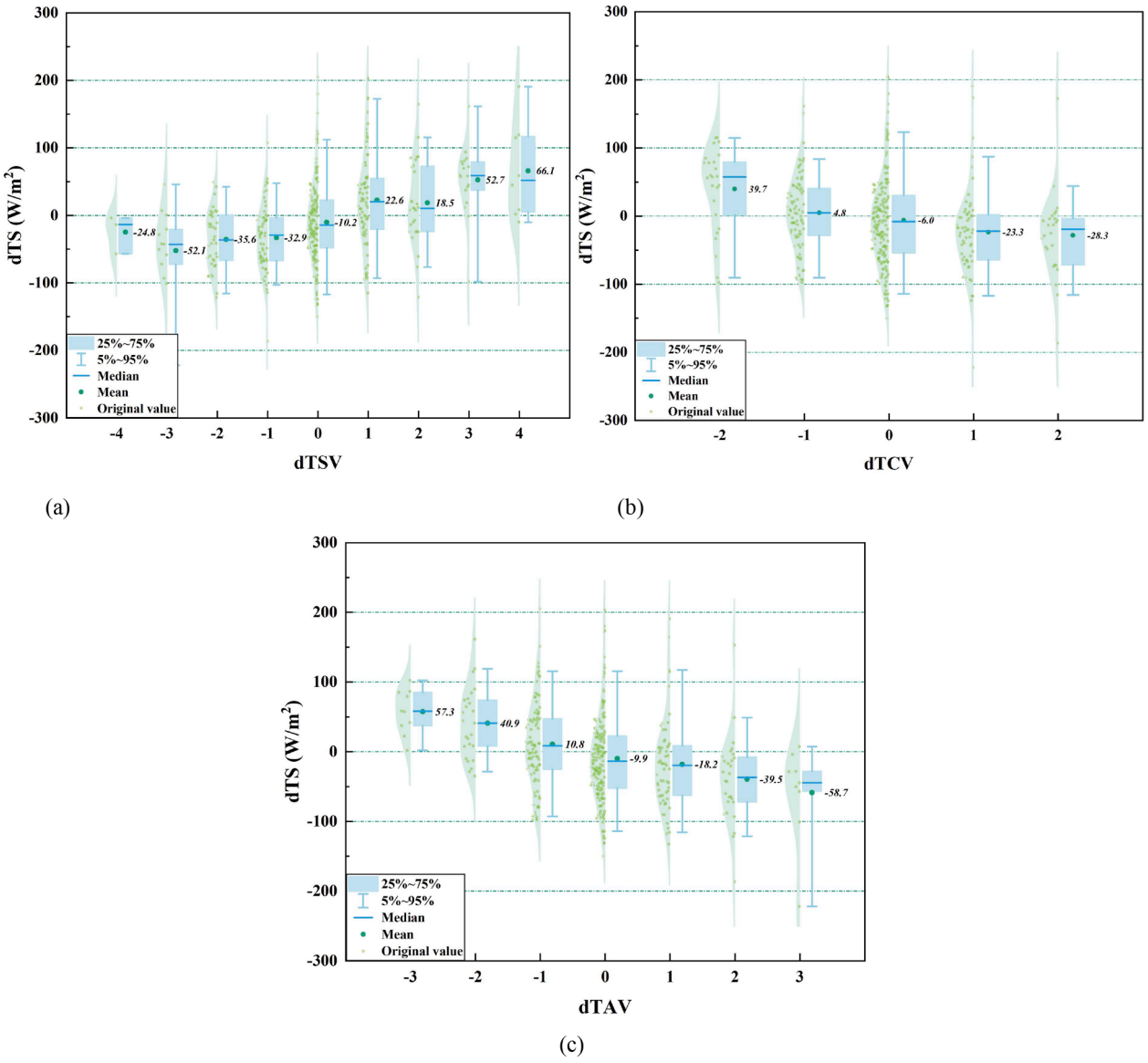

Fig. 9. Distribution of dTS under different thermal evaluations; (a) *dTSV*; (b) *dTCV* (c) *dTAV*.

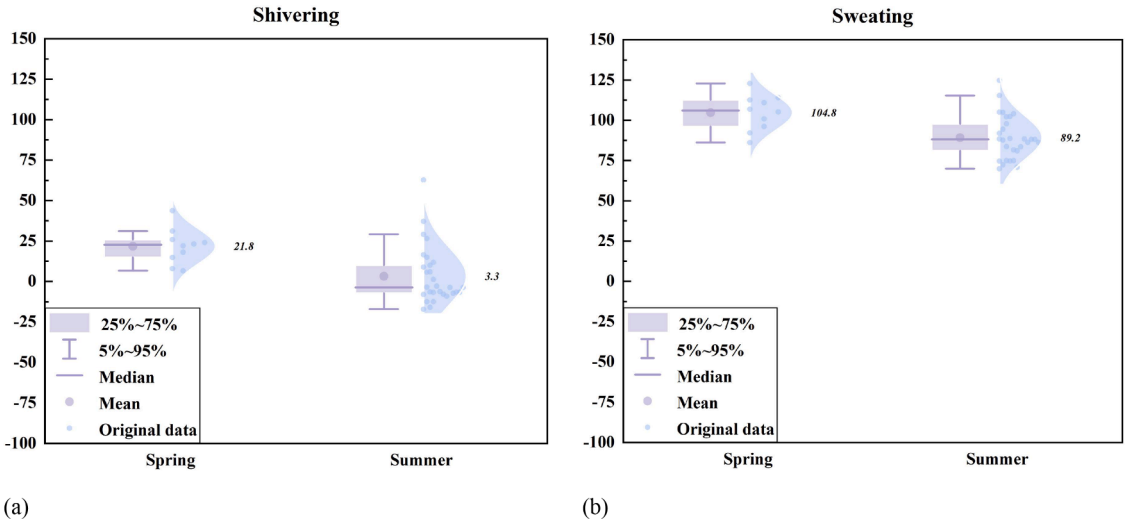

Fig. 10. Threshold of thermoneutral zone for each subject; (a) Shivering; (b) Sweating.

Table 2
Average results from *JOS-3* simulation of the threshold for thermoneutral zone.

Physiological state	Season	TS (W/m^2)	M (W/m^2)	R_S (W/m^2)	C (W/m^2)	R_L (W/m^2)	E_{sk} (W/m^2)	Q_{res} (W/m^2)
Sweating	Spring	104.82	96.96	127.10	66.67	27.63	14.12	10.80
	Summer	89.24	96.90	127.44	77.39	30.67	17.53	9.51
Shivering	Spring	21.80	96.96	127.10	121.82	50.49	15.75	14.19
	Summer	3.30	96.90	127.44	133.69	52.98	21.23	13.14

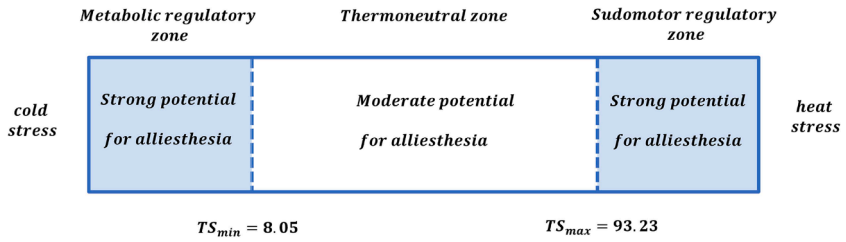

Fig. 11. The boundary and classification of thermal alliesthesia zones.

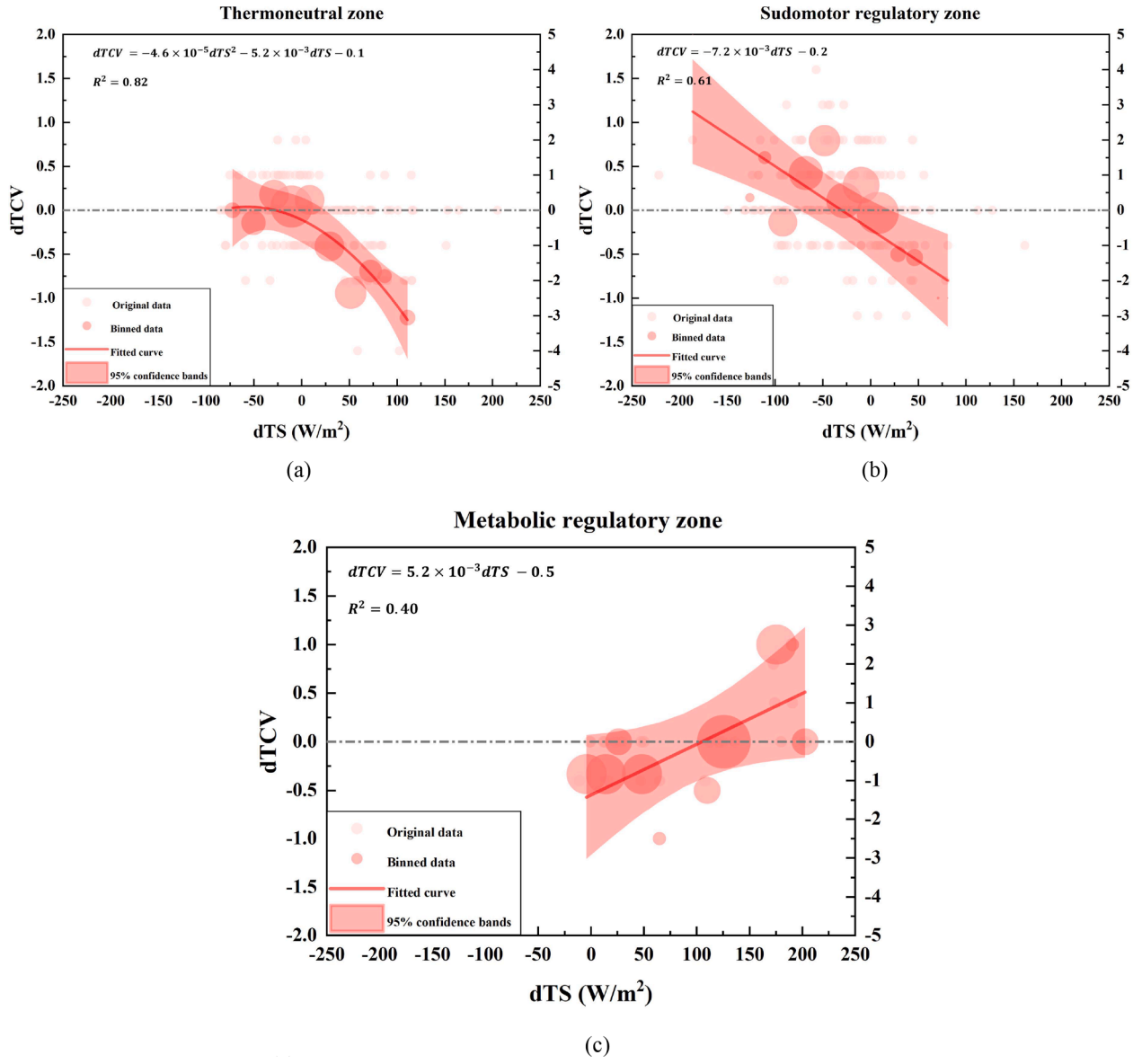

Fig. 12. The relationship between *dTS* and *dTCV*; (a) Thermoneutral zone; (b) Sudomotor regulatory zone; (c) Metabolic regulatory zone.

3.2.2. Relationship between dTS and dTCV in different alliesthesial potential zones

According to previous literature, when the same thermal stimulus is given to different zones, the amount of induced thermal comfort differs [27,43,72]. These patterns are consistent with our dataset, as shown in Fig. 12, which presents the relationships between *dTS* and *dTCV* in thermoneutral, sudomotor regulatory and metabolic regulatory zones, respectively. To account for inter-individual variability, the *dTS* data was binned in increments of 20 W/m^2 with bins containing fewer than three data points excluded to ensure statistical stability. The mean *dTCV* for each bin was then calculated and used for the subsequent regression analysis. Detailed regression statistics are provided in Table S10. Within the thermoneutral zone, there is a quadratic regression relationship between *dTS* and *dTCV* (Fig. 12 (a)). Deviations in *dTS* within this zone either maintain or reduce the *TCV* level. Specifically, a narrow *dTS* range (approximately −50 W/m^2 to −25 W/m^2) maintains *TCV* levels, whereas any increase or further decrease in *dTS* leads to a decline in *TCV*. Because the dataset contains a limited range of negative *dTS* values within the thermoneutral zone, the observed decrease in *TCV* is mainly associated with positive changes in *dTS*. The response is particularly pronounced, as an increase of approximately 50 W/m^2 in *dTS* corresponds to nearly a one-scale decrease in *TCV*. In the sudomotor regulatory zone, the relationship between *dTS* and *dTCV* follows a negative linear trend (Fig. 12 (b)). Any cooling strategies that lower overall *TS* in this zone can significantly enhance thermal comfort, with every 97 W/m^2 decrease in *dTS* corresponding to a 0.5-level increase in thermal comfort. Fig. 12 (c) presents all the data points belonging to the metabolic regulatory zone. Although the metabolic regulatory zone has a smaller dataset compared to the other two zones, it is still evident that when *dTS* is less than 95 W/m^2, the *TCV* level remains negative. Notably, a 192 W/m^2 change in *dTS* is required for every 0.5-level increase in *TCV*. By comparing Fig. 12 (b) and (c), it is noticeable that *TS* changes more readily impact *TCV* when individuals start sweating than shivering.

3.3. The impact of temporal alliesthesia on TCV

The natural thermal fluctuation along the experimental route—primarily influenced by wind and radiation levels, as discussed in Section 3.1.1—enabled the fluctuation of *TCV* through both temporal and spatial alliesthesia. The specific mechanisms of how these environmental fluctuations modulate thermal comfort perception are schematically illustrated in Fig. 13, which is a summary of the findings from the below analysis. According to this framework, urban designers are encouraged to prioritize controlled temporal variability in moderate climates to evoke positive alliesthesia, while reserving absolute mitigation strategies for periods of extreme thermal stress. Along walking routes, designers can strategically sequence spatial transitions that alternate among distinct microclimates, thereby rhythmically stimulating dynamic thermal pleasure. However, the application of spatial uniformity requires more careful consideration. Within thermoneutral zones, a uniform thermal environment is generally more desirable. In contrast, within the sudomotor regulatory zone, spatial uniformity created by natural settings has limited capacity to enhance thermal comfort, whereas mechanically induced uniformity may offer more substantial benefits.

3.3.1. Temporal alliesthesia and TCV

The overall *TS* data was binned in increments of 5 W/m^2, with bins containing fewer than three data points excluded from the analysis. Since human subjects were likely influenced by both forms of alliesthesia simultaneously, these effects could not be entirely separated. To minimize their impact on each other, data points were grouped and analyzed accordingly. For the analysis of temporal alliesthesia, data points were categorized into two groups: high temporal variation and low temporal variation. The standard deviation (*std*) and average *TS* were calculated for each route section. Borrowed from the *TI* calculation method, the temporal variation of overall *TS* was determined by dividing the *std* by the average *TS* for each route section. The median

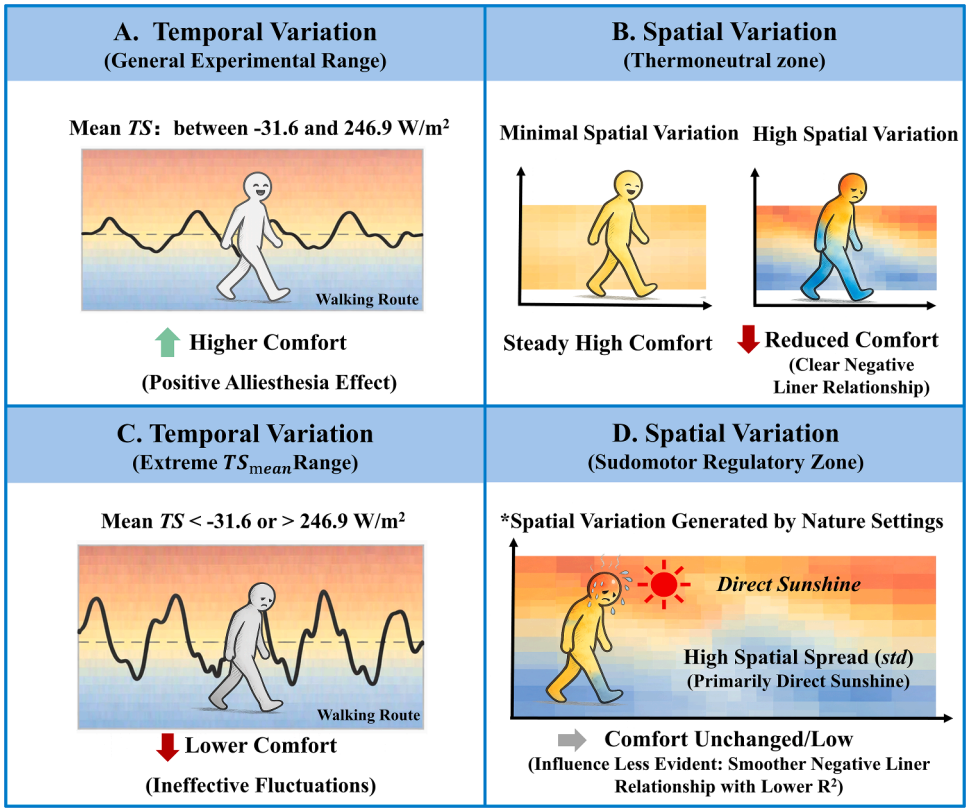

Fig. 13. Mechanism of Temporal and Spatial Alliesthesia on Thermal Comfort Variation in Fluctuating Environments.

value of this calculation (*std*/average = 0.48) was used as the cutoff point: bins with std/average < 0.48 were classified as low temporal variation, while those with std/average ≥ 0.48 were classified as high temporal variation.

Fig. 14 presents the regression results of overall *TS* and *TCV* for both groups. To account for the fact that high temporal variation along a route section does not necessarily equal high *dTS* for adjacent survey points, average *TS* and *TCV* for each route section were used in the analysis. Comparing the groups with low and high temporal variation, across the whole experimental range of TS_{mean}, the group with higher temporal variation shows a higher mean *TCV* than the group with lower temporal variation. However, when the mean TS_{mean} is lower than -31.6 W/m^2 or exceeds 246.9 W/m^2, the conclusion reverses. This may be due to the fact that the high temporal variation group with too low or too high mean *TS* indicates continuous high/low mean *TS* with transient fluctuations that last for too short a time to evoke an effective positive thermal perception response to reverse the case. This finding suggests that temporal alliesthesia along the route has considerable potential to enhance thermal comfort; however, its effect depends strongly on the intensity and duration of the thermal stimulus, which still need further investigation.

3.3.2. The influence of past TS on current TCV in different seasons

To clarify when temporal variations along the experimental route influence thermal comfort, this section analyzes the relationship between past overall *TS* and current *TCV* across different alliesthesial zones. This analysis correlates Δ*TS* along the experimental route with *TCV* to identify the time point associated with the maximum correlation coefficient. Taking the time of questionnaire submission as t_1, the current TS_{t_1} and *TCV* were obtained. *TS* values at past time points (TS_{t_0}) were obtained by tracing back 105 s from t_1 in 5 s intervals. As illustrated in Fig. 15, Δ*TS* was calculated as the difference between TS_{t_0} and TS_{t_1}. Pearson correlation analysis was performed between Δ*TS* and *TCV* to quantify their relationship at each time point. Fig. 15 also displays the Pearson correlation coefficients between Δ*TS* and *TCV* for past time points. The blue, pink and green dots represent data from three different zones. Hollow point markers represent data with *p-values* < 0.01.

Overall, Δ*TS* from the past time points has an impact on the current *TCV*, but the intensity of the impact varies. In the sudomotor regulatory zone, the correlation coefficient fluctuates around zero, alternating between positive and negative values. A significant positive correlation is observed at 20 s, where the coefficient reaches a peak of 0.19. The metabolic regulatory zone exhibits the most distinct initial variation. At 5 s, the correlation coefficient shows a sharp, significant drop to approximately -0.39, indicating the strongest negative correlation among all zones at the onset. The data in the thermoneutral zone remains relatively stable, with coefficients generally ranging between -0.2 and 0.2. However, a significant negative dip occurs at 40 s, reaching a value of -0.24, suggesting a delayed negative correlation in this zone. This indicates that *TS* variations occurring around 40 s exert the strongest influence on *TCV*, which is consistent with our previous observations [48].

3.4. The impact of spatial alliesthesia on TCV

3.4.1. Spatial alliesthesia and TCV

A similar method to the one described in Section 3.3.1 was used to analyze the effect of spatial alliesthesia on thermal comfort during outdoor walking. The spatial *TS* differences across body segments were primarily influenced by two factors: the asymmetric exposure to $R_{S_{dir}}$ and the differences in *C* due to varying clothing coverage. The spatial variation for each body segment was quantified using the *std* of all local *TS* values for each dataset. To analyze the relationship between spatial variation and thermal comfort, all original data were averaged for each route section and grouped in 2.5 W/m^2 increments, ranging from the minimum to maximum mean *TS*. The dataset was separated into two groups by the upper range of thermoneutral zone (93.23 W/m^2 shown in Fig. 11). The datapoints belonging to metabolic regulatory zones were neglected from further analysis due to limited data points. Therefore, the whole dataset was separated into thermoneutral and sudomotor regulatory zones.

It is interesting to note that our data indicate spatial alliesthesia observed in natural settings does not enhance thermal comfort perception; rather, it tends to reduce it. As shown in Fig. 16(a), spatial alliesthesia is not favored within the thermoneutral zone, where a clear negative linear relationship is identified. In other words, when human subjects remain in thermoneutral zones, they generally prefer minimal spatial thermal variation. However, in the sudomotor regulatory zone, the influence of spatial thermal differences on thermal comfort becomes less evident, as reflected by the nearly horizontal regression line along the x-axis, which represents the standard deviation of local *TS*. This may be attributed to the fact that the high *std* observed in the sudomotor regulatory zone was primarily caused by exposure to direct sunlight during the outdoor experimental route. In these natural settings, no mechanical devices were used to provide localized cooling. Further experiments are necessary to explore the effects of spatial alliesthesia induced by mechanical cooling in outdoor environments.

3.4.2. Relationship between local TS and overall TCV

To examine the distinct influence of *TS* across different body segments within each alliesthesia zone, an embedded feature selection method based on a Gradient Boosting model was applied to identify the

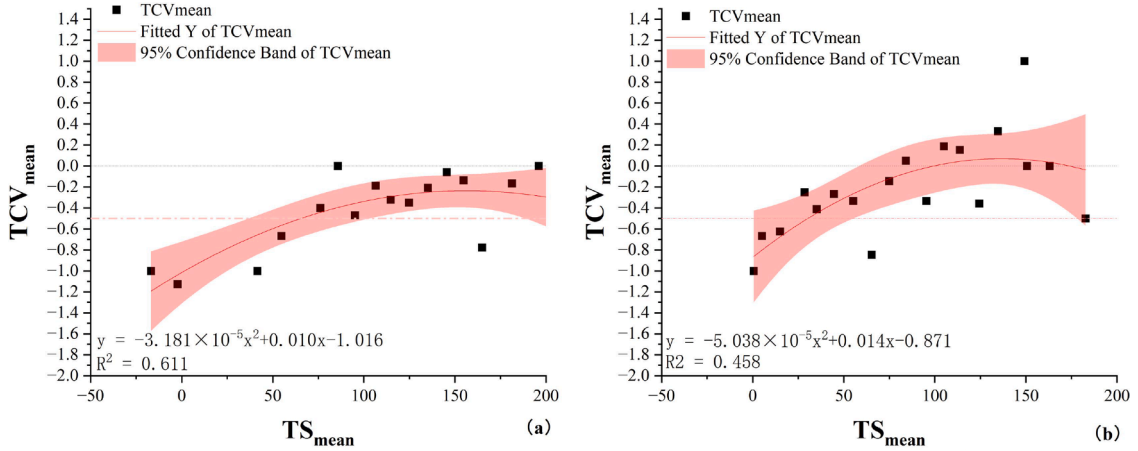

Fig. 14. Regression results for overall *TS* and *TCV*; (a) Low temporal variation (*std*/average < 0.48); (b) High temporal variation (*std*/average ≥ 0.48).

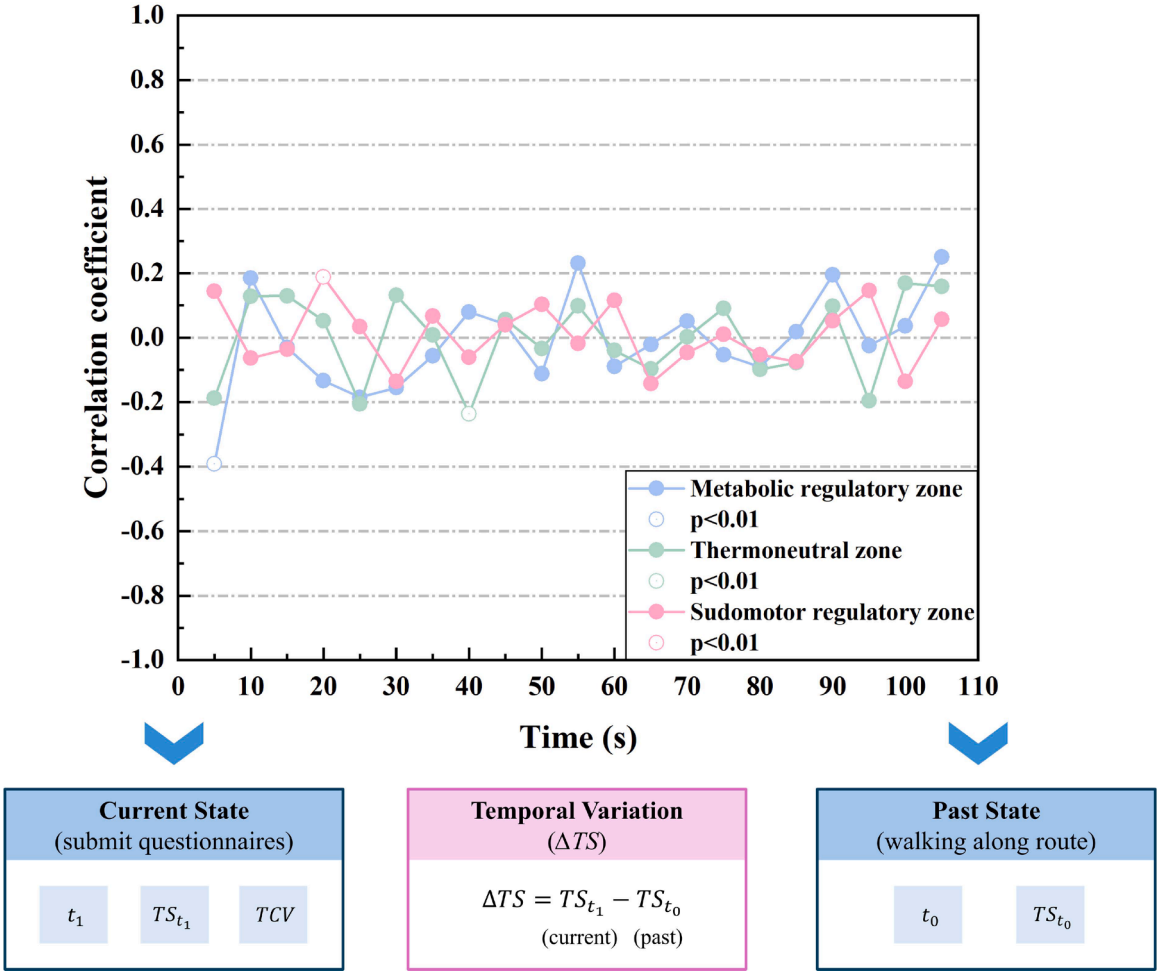

Fig. 15. Correlation coefficient at each time point for *dTS* and *TCV*.

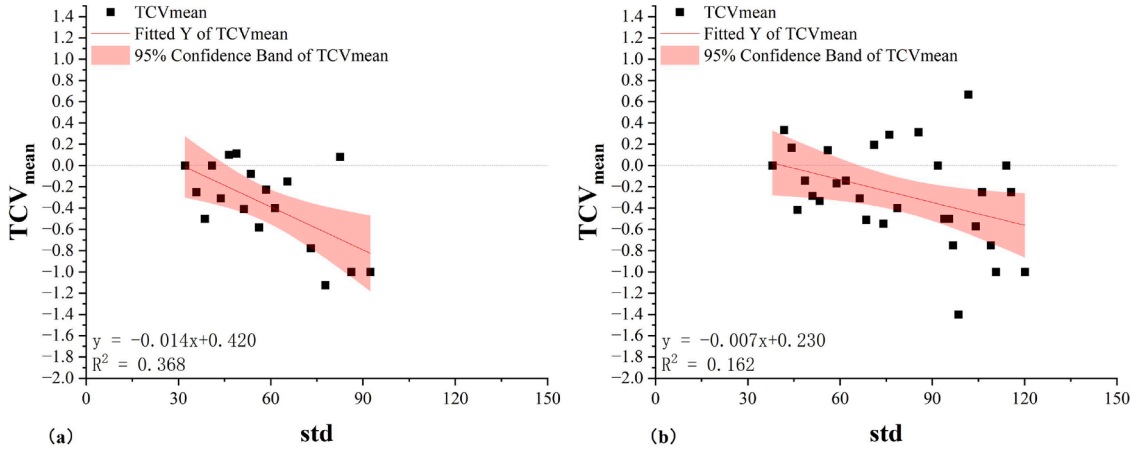

Fig. 16. Regression results for standard diviation of *TS* and *TCV*; (a) Overall *TS* in thermoneutral zone; (b) Overall *TS* in sudomotor regulatory zone.

most influential segments.

The ranking results of feature importance are shown in Fig. 17. In the metabolic regulatory zone, where the body is exposed to a cold environment, the cold exposure increases *M*, most of which is attributed to skeletal muscle contraction [73]. During walking, the legs constitute the largest muscle group, serving as the primary source of metabolic heat production while also providing a large surface area for heat loss. Consequently, *TS* changes in the legs are more readily perceived by thermoreceptors, exerting a dominant influence on overall *TCV*. In the thermoneutral zone, human thermoregulation relies mainly on vasoconstriction and vasodilation. Due to its high thermoreceptor density, the face exhibits elevated thermosensitivity [74] and exerts the strongest influence on overall *TCV*. Within the sudomotor regulatory zone, the abdomen and back play a notable role in sudomotor sensitivity [74] and show a stronger association with changes in *TCV*.

In conclusion, when human subjects are in different thermal states,

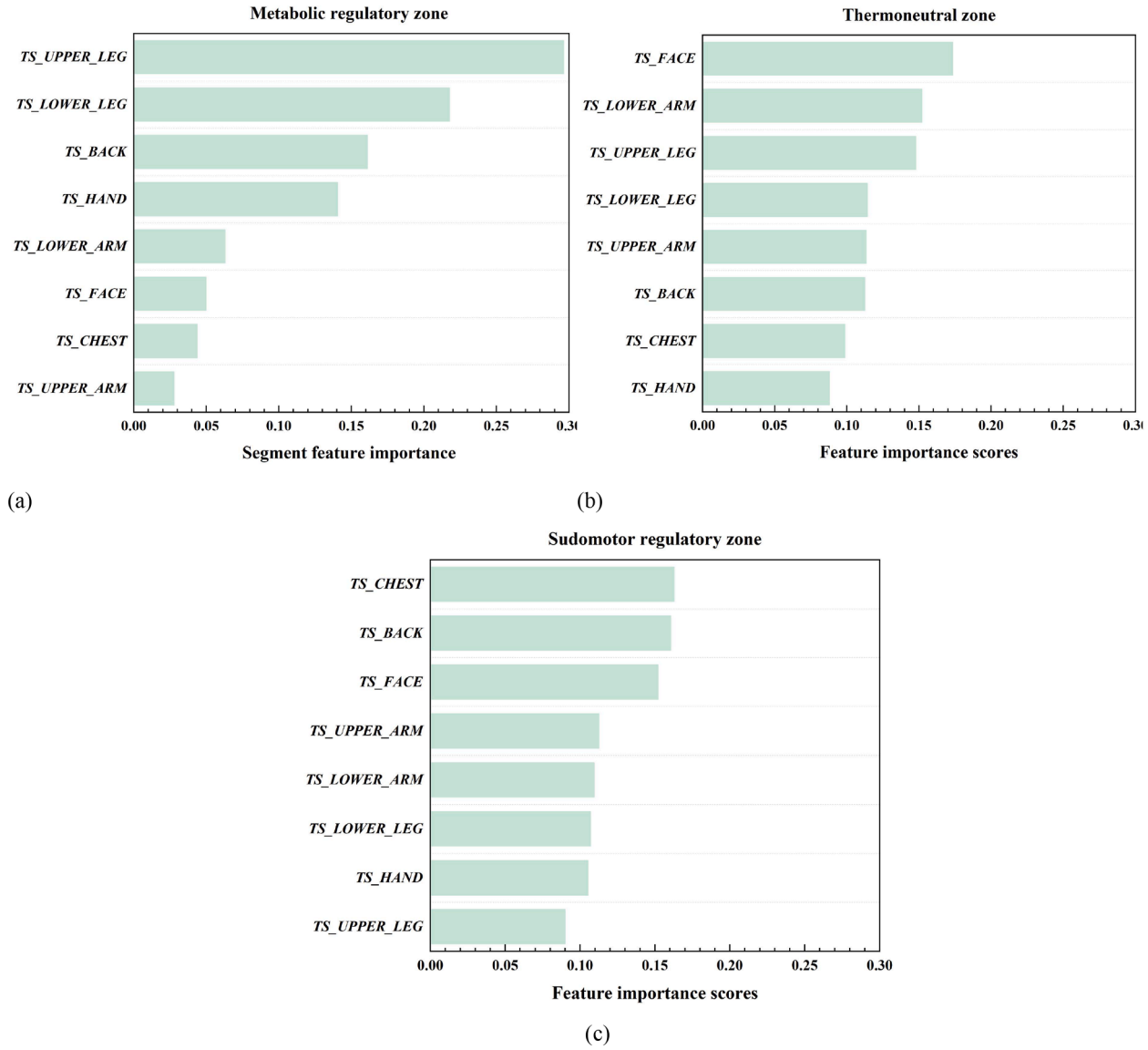

Fig. 17. The feature importance ranking of local *TS* for overall *TCV*; (a) Metabolic regulatory zone; (b) Thermoneutral zone; (c) Sudomotor regulatory zone.

the dominant body segments may vary. Accordingly, targeted modulation of local *TS* in specific body segments, such as insulating the thighs under cold stress or enhancing cooling at the back under warm conditions, may effectively improve overall *TCV*. Compared to research on resting situations (seated), it is noted that in a neutral environment, when subjects are at rest [75] or walking, the face (head) emerges as the most sensitive segment. When under warm conditions, the face was found to be the most sensitive region at rest [76], whereas the chest became the most sensitive during walking. Furthermore, in a cold environment, abdomen heating is most comfortable when resting [77]. However, while walking, heating the legs has a more significant impact on thermal comfort, providing insights into the development of personalized thermal comfort solutions for pedestrians.

4. Limitations and future work

4.1. Limitations of the study

There are still some limitations in this study. Firstly, some assumptions and simplifications are made in the calculation of *TS*. For instance, due to the limitations of experimental equipment, skin wetness data were not directly measured but simulated using the *JOS-3* model. Additionally, due to the limited number of $T_{sk,i}$ measurement points, heat gain and loss from the neck, pelvis, and foot were not considered. To address this limitation, the $T_{sk,m}$ was calculated using an eight-point method that excluded the nodes of the neck, pelvis, and foot. The heat production from these segments and the heat exchange between these three segments and the external environment were not included in the calculation. Furthermore, in the calculation of spatial *TS*, heat exchange between different body segments due to blood flow was not considered, and the heat gain and loss were assumed to occur within the same body segment. Future studies should consider measuring more physiological parameters, such as core temperature, blood pressure, heart rate, and sweat rate, and making improvements to the calculation of *TS*. Secondly, the limited data from the winter experiment hinders our analysis of thermal alliesthesia effect in the metabolic regulatory zone. Finally, it should be noted that this study focused on healthy young adults. The exclusion of vulnerable populations, such as children and the elderly, may limit the direct generalizability of the findings to broader public-space planning, as these groups may exhibit different thermoregulatory and subjective responses.

4.2. Limitations of the JOS-3 model in complex outdoor environments

Firstly, the model's isotropic radiation assumption fails to capture directional solar gradients, potentially biasing local alliesthesia assessments due to neglected segment temperature variations. Secondly, the reliance on steady-state convective coefficients overlooks outdoor turbulence and walking-induced airflow, which likely underestimates heat dissipation at the limbs. Finally, the static treatment of clothing neglects dynamic fluctuations in thermal and evaporative resistance caused by moisture accumulation, wind penetration, and color-dependent solar absorption.

5. Conclusion

This study investigated the potential of applying the thermal alliesthesia concept to enhance pedestrian thermal comfort by examining the relationship between *TS* and thermal alliesthesia. 51 subjects took part in experiments, walking along an outdoor route and stopping at 9 survey points to record their thermal perceptions. Microclimate parameters and $T_{sk,i}$ were continuously measured throughout the experiments. The boundaries of the thermoneutral zone were defined using overall *TS*, and the effects of both temporal and spatial alliesthesia on pedestrian thermal comfort were analyzed.

The main conclusions can be summarized in the following three points.

1. *The JOS-3* simulation was used to determine boundaries separating the thermoneutral zone from the metabolic regulatory zone and the sudomotor regulatory zone. These boundaries were identified as 8.05 W/m^2 (TS_{min}) and 93.23 W/m^2 (TS_{max}). In the moderate alliesthesia potential zone, the relationship between *dTS* and *dTCV* followed a quadratic regression, whereas in the strong alliesthesia potential zone, the relationship was linear. Specifically, in the sudomotor regulatory zone, they are negatively correlated, while in the metabolic regulatory zone, they exhibit a positive correlation.
2. Temporal thermal variation along the walking route can generate temporal alliesthesia, influencing *TCV*. Compared to low temporal variation, high temporal variation conditions along the route can allow higher thermal comfort level compared to low temporal variation conditions within the range of -31.6 W/m^2 to 246.9 W/m^2 for mean *TS*. The influence of short-term thermal history (past *TS* variation) on current *TCV* varied, with the strongest impact observed at at a lag of 20 s in sudomotor regulatory zone, 40 s in thermoneutral zone, and 5 s in metabolic regulatory zone.
3. Spatial variation across different body segments can induce spatial alliesthesia, influencing pedestrians' *TCV*. Spatial alliesthesia is not favored by human subjects in thermoneutral zone: an increase of local *TS* difference can lead to a noticeable decrease in thermal comfort level. But its effect is less obvious in the sudomotor regulatory zone. When individuals are in different thermal states, the dominant body segments may vary. In the strong potential of alliesthesia zone, the most sensitive segments are back, chest and legs, while in moderate potential of alliesthesia zone, the most sensitive segment is face.

CRediT authorship contribution statement

Yichun Li: Writing – original draft, Visualization, Software, Methodology, Investigation, Formal analysis, Data curation. **Xianzhun Zhong:** Software, Methodology. **Yongxin Xie:** Writing – review & editing, Validation, Supervision, Resources, Project administration, Funding acquisition, Conceptualization. **Richard de Dear:** Writing – review & editing, Validation, Supervision. **Shuai Lu:** Writing – review & editing. **Borong Lin:** Writing – review & editing. **Jianlei Niu:** Writing – review & editing, Supervision, Funding acquisition.

Declaration of competing interest

The authors declare that they have no known competing financial interests or personal relationships that could have appeared to influence the work reported in this paper.

Acknowledgments

The work was supported by National Natural Science Foundation of China (Project No. 52308121) and Research Grants Council of the Hong Kong Special Administrative Region, China, Theme-based Research Scheme (Project No. T22-504/21-R). We would like to thank Miss Jianxiu Wen and Miss Xinyi Wang for their help during the data collection process.

Supplementary materials

Supplementary material associated with this article can be found, in the online version, at doi:10.1016/j.buildenv.2026.114434.

Data availability

Data will be made available on request.

References

[1] L. Chen, C.M. Mak, J. Hang, Y. Dai, Influence of elevated walkways on outdoor thermal comfort in hot-humid climates based on on-site measurement and CFD modeling, Sustain. Cities. Soc. 100 (2024) 105048, https://doi.org/10.1016/j.scs.2023.105048. /01/01/2024.
[2] C.C. Marcus, C. Francis, People places: Design Guidlines For Urban Open Space, John Wiley & Sons, 1997.
[3] L. Chen, E. Ng, Outdoor thermal comfort and outdoor activities: A review of research in the past decade, Cities. 29 (2) (2012) 118–125.
[4] R. Basu, N. Colaninno, A. Alhassan, A. Sevtsuk, Hot and bothered: exploring the effect of heat on pedestrian route choice behavior and accessibility, Cities. 155 (2024) 105435, https://doi.org/10.1016/j.cities.2024.105435. /12/01/2024.
[5] S. Mohite, M. Surawar, Impact of urban street geometry on outdoor pedestrian thermal comfort during heatwave in Nagpur city, Sustain. Cities. Soc. 108 (2024) 105450, https://doi.org/10.1016/j.scs.2024.105450. /08/01/2024.
[6] I. Azcarate, J.Á. Acero, L. Garmendia, E. Rojí, Tree layout methodology for shading pedestrian zones: thermal comfort study in Bilbao (Northern Iberian Peninsula), Sustain. Cities. Soc. 72 (2021) 102996, https://doi.org/10.1016/j.scs.2021.102996. /09/01/2021.
[7] T. Liu, et al., Investigating the impact of a large river and its surrounding contextual conditions on pedestrians' summer thermal perceptions in a Cfa-climate city, Sci. Rep. 14 (1) (2024) 13833, https://doi.org/10.1038/s41598-024-64729-7, 2024/06/15.
[8] S. Jia, Y. Wang, N.H. Wong, W. Chen, X. Ding, Influences of the thermal environment on pedestrians' thermal perception and travel behavior in hot weather, Build. Environ. 226 (2022) 109687, https://doi.org/10.1016/j.buildenv.2022.109687, 2022/12/01/.
[9] B. Choudhary, Udayraj, A modified multi-node human thermoregulation model with improved sweating response to simulate human physiological behaviours in warm and hot environments, Build. Environ. 267 (2025) 112164, https://doi.org/10.1016/j.buildenv.2024.112164. /01/01/2025.
[10] Y. Zhang, Z. Zheng, S. Zhang, Z. Fang, Z. Lin, Exploring thermal comfort and pleasure in outdoor shaded spaces: inspiration for improving thermal index models, Build. Environ. 265 (2024) 111933, https://doi.org/10.1016/j.buildenv.2024.111933, 2024/11/01/.
[11] C. Vasilikou, M. Nikolopoulou, Outdoor thermal comfort for pedestrians in movement: thermal walks in complex urban morphology, Int. J. Biometeorol. 64 (2) (2020) 277–291, https://doi.org/10.1007/s00484-019-01782-2, 2020/02/01.
[12] O. Jay, et al., Reducing the health effects of hot weather and heat extremes: from personal cooling strategies to green cities, Lancet 398 (10301) (2021) 709–724, https://doi.org/10.1016/S0140-6736(21)01209-5, 2021/08/21/.
[13] A.S.H. Abdallah, R.M.A. Mahmoud, Urban morphology as an adaptation strategy to improve outdoor thermal comfort in urban residential community of new assiut city, Egypt, Sustain. Cities. Soc. 78 (2022) 103648, https://doi.org/10.1016/j.scs.2021.103648, 2022/03/01/.
[14] F. Peng, Y. Xiong, B. Zou, Identifying the optimal travel path based on shading effect at pedestrian level in cool and hot climates, Urban. Clim. 40 (2021) 100988, https://doi.org/10.1016/j.uclim.2021.100988, 2021/12/01/.
[15] B. Abdi, A. Hami, D. Zarehaghi, Impact of small-scale tree planting patterns on outdoor cooling and thermal comfort, Sustain. Cities. Soc. 56 (2020) 102085.
[16] B.M. de Quadros, M.G.O. Mizgier, Urban green infrastructures to improve pedestrian thermal comfort: A systematic review, Urban. For. Urban. Green. 88 (2023) 128091, https://doi.org/10.1016/j.ufug.2023.128091, 2023/10/01/.

[17] T.R. Oke, Boundary Layer Climates, Routledge, 2002.
[18] H. Du, X. Song, H. Jiang, Z. Kan, Z. Wang, Y. Cai, Research on the cooling island effects of water body: A case study of Shanghai, China, Ecol. Indic. 67 (2016) 31–38, https://doi.org/10.1016/j.ecolind.2016.02.040, 2016/08/01/.
[19] H. Zhao, G. Xu, Y. Shi, Y. Zhai, L. Zhao, R.D. Brown, Evaluation of pedestrian thermal comfort from a whole-trip perspective: an outdoor empirical study, Sustain. Cities. Soc. 115 (2024) 105872, https://doi.org/10.1016/j.scs.2024.105872, 2024/11/15/.
[20] A.Y. Abdelmejeed, D. Gruehn, Pedestrian dynamic thermal comfort analysis to optimize using trees in various urban morphologies: A case study of Cairo City, Land. (Basel) 13 (9) (2024) 1489 [Online]Available: https://www.mdpi.com/2073-445X/13/9/1489.
[21] H. Zhao, et al., The impact of dynamic thermal experiences on pedestrian thermal comfort: A whole-trip perspective from laboratory studies, Build. Environ. 258 (2024) 111599, https://doi.org/10.1016/j.buildenv.2024.111599, 2024/06/15/.
[22] Y. Sang, et al., Dynamic changes of urban street thermal environment from the pedestrian perspective and their impacts on pedestrians' walking behaviors, Sustain. Cities. Soc. 135 (2025) 106971, https://doi.org/10.1016/j.scs.2025.106971, 2025/12/15/.
[23] X. Ma, T. Zeng, R. de Dear, Y. Xie, C. Yuan, S. Lu, Active route choice to minimize pedestrian thermal discomfort in a high-density subtropical city, Sustain. Cities. Soc. 131 (2025) 106697, https://doi.org/10.1016/j.scs.2025.106697, 2025/09/01/.
[24] B. Huang, A. Matzarakis, B.-J. He, Nonlinear law of cumulative heat exposure and dynamic thermal comfort during pedestrians' walking: field experiments and machine learning predictions, Sustain. Cities. Soc. 131 (2025) 106696, https://doi.org/10.1016/j.scs.2025.106696, 2025/09/01/.
[25] H. Zhao, W. Ji, S. Deng, Z. Wang, S. Liu, A review of dynamic thermal comfort influenced by environmental parameters and human factors, Energy Build. 318 (2024) 114467, https://doi.org/10.1016/j.enbuild.2024.114467, 2024/09/01/.
[26] H. Liu, M. He, Y. Wu, M. Liu, B. Li, Dual effect of activity levels and temperature step-change on human comfort and recovery time: simulated short-term commute in winter, Build. Environ. 247 (2024) 111034, https://doi.org/10.1016/j.buildenv.2023.111034, 2024/01/01/.
[27] Y. Jiang, Y. Xie, J. Niu, Short-term dynamic thermal perception and physiological response to step changes between real-life indoor and outdoor environments, Build. Environ. 251 (2024) 111223, https://doi.org/10.1016/j.buildenv.2024.111223, 2024/03/01/.
[28] M. Vellei, I. Pigliautile, A.L. Pisello, Effect of time-of-day on human dynamic thermal perception, Sci. Rep. 13 (1) (2023) 2367, https://doi.org/10.1038/s41598-023-29615-8, 2023/02/09.
[29] M. Cabanac, Physiological role of pleasure: A stimulus can feel pleasant or unpleasant depending upon its usefulness as determined by internal signals, Science (1979) 173 (4002) (1971) 1103–1107.
[30] R. De Dear, Revisiting an old hypothesis of human thermal perception: alliesthesia, Build. Res. Inf. 39 (2) (2011) 108–117.
[31] T. Parkinson, R. De Dear, Thermal pleasure in built environments: physiology of alliesthesia, Build. Res. Inf. 43 (3) (2015) 288–301.
[32] T. Parkinson, R. de Dear, C. Candido, Thermal pleasure in built environments: alliesthesia in different thermoregulatory zones, Build. Res. Inf. 44 (1) (2016) 20–33.
[33] T. Parkinson, R. de Dear, Thermal pleasure in built environments: spatial alliesthesia from contact heating, Build. Res. Inf. 44 (3) (2016) 248–262.
[34] T. Parkinson, R. de Dear, Thermal pleasure in built environments: spatial alliesthesia from air movement, Build. Res. Inf. 45 (3) (2017) 320–335.
[35] R. Rawal, M. Schweiker, O.B. Kazanci, V. Vardhan, Q. Jin, and L. Duanmu, Personal comfort systems: A review on comfort, energy, and economics, *energy and buildings*, vol. 214, p. 109858, 2020/05/01/2020, doi: https://doi.org/10.1016/j.enbuild.2020.109858.
[36] Y. He, et al., Creating alliesthesia in cool environments using personal comfort systems, Build. Environ. 209 (2022) 108642, https://doi.org/10.1016/j.buildenv.2021.108642, 2022/02/01/.
[37] Y. Watanabe, et al., Thermal perception of infrared radiation applied at different wavelengths to distal body segments in neutral and cool ambient environments, Build. Environ. 262 (2024) 111783, https://doi.org/10.1016/j.buildenv.2024.111783, 2024/08/15/.
[38] M.A. Belyamani, et al., Local wearable cooling may improve thermal comfort, emotion, and cognition, Build. Environ. 254 (2024) 111367, https://doi.org/10.1016/j.buildenv.2024.111367, 2024/04/15/.
[39] S. Liu, N. Nazarian, J. Niu, M.A. Hart, R. de Dear, From thermal sensation to thermal affect: A multi-dimensional semantic space to assess outdoor thermal comfort, Build. Environ. 182 (2020) 107112, https://doi.org/10.1016/j.buildenv.2020.107112, 2020/09/01/.
[40] Y. Dzyuban, et al., Evidence of alliesthesia during a neighborhood thermal walk in a hot and dry city, Sci. Total Environ. 834 (2022) 155294.
[41] S.A Smail, N. Zemmouri, M. Djenane, M. Nikolopoulou, Investigating the transient conditions of "Sabat" space and its influence on pedestrian sensations during thermal walks. Algiers' Casbah case study, Build. Environ. 261 (2024) 111760, https://doi.org/10.1016/j.buildenv.2024.111760, 2024/08/01/.
[42] S. Shooshtarian, Theoretical dimension of outdoor thermal comfort research, Sustain. Cities. Soc. 47 (2019) 101495.
[43] S. Liu, N. Nazarian, M.A. Hart, J. Niu, Y. Xie, R. de Dear, Dynamic thermal pleasure in outdoor environments-temporal alliesthesia, Sci. Total Environ. 771 (2021) 144910.
[44] N. Bema and B. Ozarisoy, Investigation of ASHRAE Global Thermal Comfort Database II and its impact on the development of effective passive design systems, 2023.
[45] Y. Xie, et al., Outdoor thermal sensation and logistic regression analysis of comfort range of meteorological parameters in Hong Kong, Build. Environ. 155 (2019) 175–186, https://doi.org/10.1016/j.buildenv.2019.03.035, 2019/05/15/.
[46] A. Hassani, B. Jancewicz, M. Wrotek, F. Chwałczyk, N. Castell, Understanding thermal comfort expectations in older adults: the role of long-term thermal history, Build. Environ. 263 (2024) 111900, https://doi.org/10.1016/j.buildenv.2024.111900, 2024/09/01/.
[47] Y. Shimazaki, A. Yoshida, R. Suzuki, T. Kawabata, D. Imai, S. Kinoshita, Application of human thermal load into unsteady condition for improvement of outdoor thermal comfort, Build. Environ. 46 (8) (2011) 1716–1724.
[48] Y. Xie, et al., Experimental study and theoretical discussion of dynamic outdoor thermal comfort in walking spaces: effect of short-term thermal history, Build. Environ. 216 (2022) 109039.
[49] Ashrae., 2005 ASHRAE handbook: Fundamentals, ASHRAE, 2005.
[50] A.P. Gagge, Y. Nishi, Heat exchange between human skin surface and thermal environment, Compr. Physiol. (1977) 69–92.
[51] D. Bois, A formula to estimate the approximate surface area if height and weight be known, 1916, Nutrition 5 (1989) 303.
[52] Y. Takahashi, et al., Thermoregulation model JOS-3 with new open source code, Energy Build. 231 (2021) 110575.
[53] L.B. Rowell, G. Brengelmann, J. Murray, K. Kraning 2nd, F. Kusumi, Human metabolic responses to hyperthermia during mild to maximal exercise, J. Appl. Physiol. 26 (4) (1969) 395–402.
[54] B. Saltin, A.P. Gagge, U. Bergh, J. Stolwijk, Body temperatures and sweating during exhaustive exercise, J. Appl. Physiol. 32 (5) (1972) 635–643.
[55] A.M. Roza, H.M. Shizgal, The Harris Benedict equation reevaluated: resting energy requirements and the body cell mass, Am. J. Clin. Nutr. 40 (1) (1984) 168–182.
[56] J.A. Harris, F.G. Benedict, A biometric study of human basal metabolism, Proc. Natl. Acad. Sci. 4 (12) (1918) 370–373.
[57] F. Joint, W. H. Organization, Energy and Protein requirements: Report of a Joint FAO, World Health Organization, 1973.
[58] Y. Yan, Y. Xu, S. Yue, A high-spatial-resolution dataset of human thermal stress indices over South and East Asia, Sci. Data 8 (1) (2021) 229.
[59] D. Lai, X. Zhou, Q. Chen, Measurements and predictions of the skin temperature of human subjects on outdoor environment, Energy Build. 151 (2017) 476–486, https://doi.org/10.1016/j.enbuild.2017.07.009, 2017/09/15/.
[60] S. Liu, Y. Xie, Y. Zhu, and B. Cao, From physiological stress to sustainable design: defining solar radiation tolerance thresholds for outdoor thermal comfort, *Available at SSRN 5251208*.
[61] K. Kubaha, D. Fiala, J. Toftum, A. Taki, Human projected area factors for detailed direct and diffuse solar radiation analysis, Int. J. Biometeorol. 49 (2) (2004) 113–129.
[62] D. Lai, Modeling Thermal Comfort in Outdoor Environments, Purdue University, 2017.
[63] Y. Tang, Z. Su, H. Yu, K. Zhang, C. Li, H. Ye, A database of clothing overall and local insulation and prediction models for estimating ensembles' insulation, Build. Environ. 207 (2022) 108418, https://doi.org/10.1016/j.buildenv.2021.108418, 2022/01/01/.
[64] J. Lin, Y. Jiang, Y. Xie, J. Niu, A novel method for local clothing insulation prediction to support sustainable building and urban design, (in eng), Int. J. Biometeorol. 69 (8) (Aug 2025) 1899–1917, https://doi.org/10.1007/s00484-025-02934-3.
[65] Y. Yu, J. Liu, K. Chauhan, R. de Dear, J. Niu, Experimental study on convective heat transfer coefficients for the human body exposed to turbulent wind conditions, Build. Environ. 169 (2020) 106533.
[66] R.J. De Dear, E. Arens, Z. Hui, M. Oguro, Convective and radiative heat transfer coefficients for individual human body segments, Int. J. Biometeorol. 40 (1997) 141–156.
[67] X. Jia, S. Li, Y. Zhu, W. Ji, B. Cao, Transient thermal comfort and physiological responses following a step change in activity status under summer indoor environments, Energy Build. 285 (2023) 112918, https://doi.org/10.1016/j.enbuild.2023.112918, 2023/04/15/.
[68] J.A. Stolwijk, A mathematical model of physiological temperature regulation in man, NASA (1971).
[69] P. Virtanen, et al., SciPy 1.0: fundamental algorithms for scientific computing in Python, Nat. Methods 17 (3) (2020) 261–272, https://doi.org/10.1038/s41592-019-0686-2, 2020/03/01.
[70] A. Natekin, A. Knoll, Gradient boosting machines, a tutorial, Front. Neurorobot. 7 (2013) 21.
[71] S.L. Heathcote, P. Hassmén, S. Zhou, C.J. Stevens, Passive heating: reviewing practical heat acclimation strategies for endurance athletes, (in eng), Front. Physiol. 9 (2018) 1851, https://doi.org/10.3389/fphys.2018.01851.
[72] G.D. Mower, Perceived intensity of peripheral thermal stimuli is independent of internal body temperature, J. Comp. Physiol. Psychol. 90 (12) (1976) 1152.
[73] J.W. Castellani, A.J. Young, Human physiological responses to cold exposure: acute responses and acclimatization to prolonged exposure, Autonom. Neurosci. 196 (2016) 63–74, https://doi.org/10.1016/j.autneu.2016.02.009, 2016/04/01/.
[74] J. Cotter, N. Taylor, The distribution of cutaneous sudomotor and alliesthesial thermosensitivity in mildly heat-stressed humans: an open-loop approach, J. Physiol. 565 (2005) 335–345, https://doi.org/10.1113/jphysiol.2004.081562, 06/01.
[75] W. Luo, R. Kramer, Y. de Kort, W. van Marken Lichtenbelt, Effectiveness of personal comfort systems on whole-body thermal comfort – A systematic review on

which body segments to target, Energy Build. 256 (2022) 111766, https://doi.org/10.1016/j.enbuild.2021.111766, 2022/02/01/.
[76] M. Nakamura, et al., Regional differences in temperature sensation and thermal comfort in humans, (in eng), J. Appl. Physiol. 1985 105 (6) (Dec 2008) 1897–1906, https://doi.org/10.1152/japplphysiol.90466.2008.
[77] M. Nakamura, et al., Relative importance of different surface regions for thermal comfort in humans, (in eng), Eur. J. Appl. Physiol. 113 (1) (Jan 2013) 63–76, https://doi.org/10.1007/s00421-012-2406-9.